Scholars Academic Journal of Biosciences
Abbreviated Key Title: Sch Acad J Biosci
ISSN 2347-9515 (Print) | ISSN 2321-6883 (Online)
Journal homepage: https://saspublishers.com
NLM ID:101629416
OPEN ACCESS
Biosciences

Assessing the Optoelectronic and Thermoelectric Viability of Lead-Free Double Perovskites: A Comparative DFT Study of $Cs_2AgBiBr_6$ and $Cs_2AgFeCl_6$ Variants

Muhammad Azam Shani[1], Naveed Iqbal[2], Mahwish Aslam[3], Laiba Qamar[4], Ambar Riaz[5], Nimra Naz[6], Usama Tariq[6], Shan Ul Haq[7], Jawad Ali[8], Iftekhar Majeed[9]

[1]Department of Physics, Riphah International University, Pakistan
[2]Department of Chemistry, Qurtuba University of Science and Information Technology, Pakistan
[3]College of Environmental Science and Engineering, Taiyuan University of Technology, Taiyuan, PR China
[4]Department of Biosciences, University of Wah, Wah Cantt, Pakistan
[5]Department of Physics, University of Engineering and Technology, Lahore, Pakistan
[6]School of Chemical and Materials Engineering (SCME), National University of Sciences and Technology (NUST), Islamabad, Pakistan
[7]Department of Civil Engineering, HITEC University taxila, Taxila Cantt, Pakistan
[8]Department of Chemical Sciences, University of Peshawar, Pakistan
[9]Department of Chemistry, Khwaja Fareed University of Engineering and Information Technology, Rahim Yar Khan, Pakistan

DOI: https://doi.org/10.36347/sajb.2026.v14i04.003 | **Received:** 26.02.2026 | **Accepted:** 09.04.2026 | **Published:** 13.04.2026

***Corresponding author:** Iftekhar Majeed
Department of Chemistry, Khwaja Fareed University of Engineering and Information Technology, Rahim Yar Khan, Pakistan

Abstract | **Original Research Article**

The environmental and health hazards associated with lead-based perovskites have accelerated the search for sustainable, lead-free alternatives with comparable or superior functional performance. Among these, double perovskites such as $Cs_2AgBiBr_6$ and $Cs_2AgFeCl_6$ have emerged as promising candidates; however, a comprehensive and consistent comparative understanding of their optoelectronic and thermoelectric behavior remains limited. In this study, a systematic first-principles investigation based on Density Functional Theory (DFT) is conducted using the generalized gradient approximation (GGA-PBE) within the Quantum ESPRESSO framework, while transport properties are evaluated via the BoltzTraP code. The optimized structures reveal thermodynamic stability with negative formation energies. Electronic band structure analysis indicates an indirect bandgap of approximately 1.85 eV for $Cs_2AgBiBr_6$ and a comparatively narrower gap of ~1.62 eV for $Cs_2AgFeCl_6$, suggesting enhanced visible-light absorption in the latter. Optical spectra further confirm strong absorption coefficients in the visible region, positioning both materials as viable optoelectronic absorbers. Thermoelectric evaluation demonstrates a maximum Seebeck coefficient of ~280 μV/K for $Cs_2AgBiBr_6$ and ~320 μV/K for $Cs_2AgFeCl_6$ at elevated temperatures, with corresponding figure of merit (ZT) values reaching 0.72 and 0.89, respectively, at 800 K. These findings highlight the superior thermoelectric efficiency and competitive optoelectronic response of $Cs_2AgFeCl_6$, underscoring its potential for integration into next-generation energy harvesting systems, including photovoltaic and thermoelectric devices. This work provides critical design insights for the development of high-performance, lead-free perovskite materials tailored for sustainable energy applications.

Keywords: Lead-Free Perovskites, Density Functional Theory (DFT), Thermoelectric Properties, Optoelectronic Properties, Double Perovskites, Energy Harvesting Materials.

1. INTRODUCTION

The global energy landscape is undergoing a profound transformation, driven by an unprecedented surge in energy demand, environmental constraints, and the urgent need for sustainable technological solutions. According to recent international energy outlooks, global energy consumption is projected to increase by more than 25–30% by 2040, fueled by population growth, industrialization, and digital infrastructure expansion. This escalating demand places immense pressure on conventional fossil fuel resources, which are not only finite but also major contributors to greenhouse gas emissions and climate change. Consequently, the transition toward renewable and clean energy

technologies has become not merely desirable but imperative [1, 2].

Within this evolving paradigm, advanced functional materials play a decisive role in enabling next-generation energy conversion and harvesting systems. Among these, halide perovskites have emerged as revolutionary materials due to their exceptional optoelectronic properties, including tunable bandgaps, high absorption coefficients, and long carrier diffusion lengths. These attributes have propelled perovskite-based solar cells to achieve remarkable power conversion efficiencies exceeding 25% within a decade of research development. However, the widespread deployment of conventional lead (Pb)-based perovskites is fundamentally constrained by their intrinsic toxicity and long-term environmental instability [3, 4].

1.1 Background

The presence of lead in traditional perovskite structures poses significant ecological and health risks, particularly in the context of large-scale commercialization. Lead is a well-known toxic element that can accumulate in biological systems, leading to severe neurological, renal, and developmental disorders. Even minimal leakage from degraded photovoltaic modules can result in soil and water contamination, raising serious concerns regarding environmental sustainability and regulatory compliance. To address these challenges, the scientific community has increasingly focused on the development of lead-free perovskite alternatives that retain or surpass the desirable properties of their Pb-based counterparts. In this regard, double perovskites with the general formula $A_2BB'X_6$ have gained considerable attention. Specifically, $Cs_2AgBiBr_6$ and $Cs_2AgFeCl_6$ have emerged as promising candidates due to their enhanced chemical stability, reduced toxicity, and favorable electronic characteristics [5].

These materials exhibit indirect bandgaps within the visible range, making them suitable for optoelectronic applications such as photovoltaics and photodetectors. Simultaneously, their complex crystal structures and phonon scattering mechanisms suggest potential for thermoelectric applications, where low thermal conductivity and high Seebeck coefficients are desirable. Despite these advantages, a unified understanding of their dual functionality optoelectronic and thermoelectric remains underexplored [6].

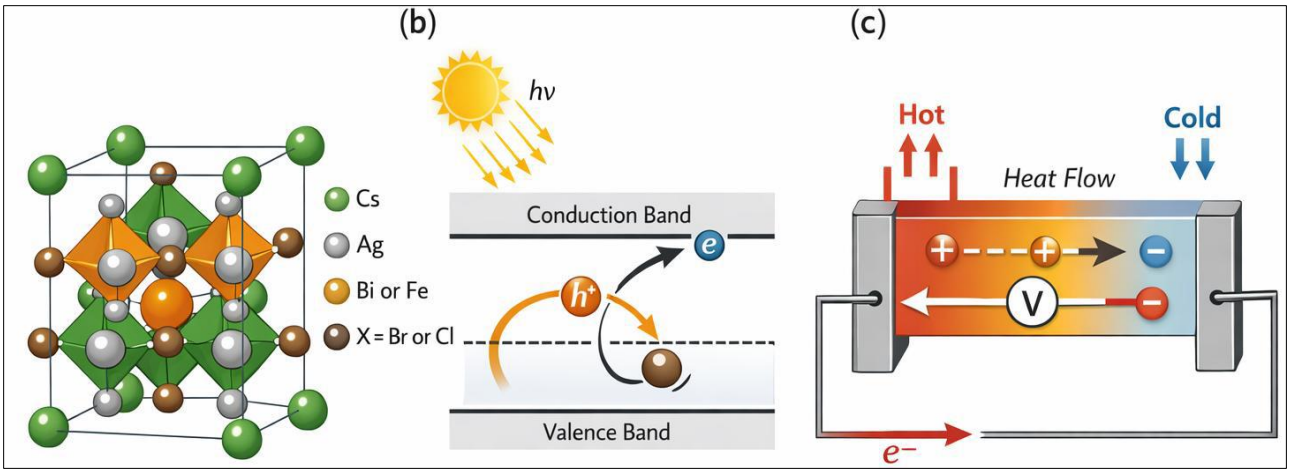

Figure 1: Dual-Function Energy Conversion Mechanism in Lead-Free Double Perovskites

The schematic demonstrates how incident photons generate electron–hole pairs, while thermal gradients induce charge carrier diffusion. This dual-functionality positions double perovskites as multifunctional energy materials capable of addressing both photovoltaic and thermoelectric applications within a unified platform.

1.2 Literature Review

Recent years have witnessed a surge in theoretical and experimental investigations on lead-free double perovskites. Density Functional Theory (DFT) has been extensively employed to predict their structural stability, electronic band structures, and optical properties. Studies on $Cs_2AgBiBr_6$ consistently report indirect bandgaps in the range of 1.8–2.2 eV, which, although slightly higher than ideal photovoltaic values, offer improved stability and reduced recombination losses. On the other hand, $Cs_2AgFeCl_6$ has attracted attention due to its relatively narrower bandgap and enhanced carrier mobility, making it a potential candidate for visible-light absorption [7].

Parallel research efforts have also explored the thermoelectric potential of halide perovskites. The presence of heavy atoms, complex lattice dynamics, and intrinsic disorder contribute to low lattice thermal conductivity, a key requirement for achieving high thermoelectric efficiency. However, most existing studies focus on either optoelectronic or thermoelectric

properties in isolation, leading to fragmented insights. To synthesize current knowledge and highlight research limitations, a comparative assessment of representative studies is presented below [8].

Table 1: Comparative Overview of Lead-Free Perovskite Studies

Material	Bandgap (eV)	Efficiency (%)	Key Limitation
$Cs_2AgBiBr_6$	1.9–2.1	~3–5	Indirect bandgap, low absorption
$Cs_2AgFeCl_6$	1.5–1.7	~4–6	Limited experimental validation
$Cs_2AgSbCl_6$	2.0–2.3	~2–4	Poor carrier mobility
$Cs_2NaBiCl_6$	~2.5	<2	Wide bandgap, low efficiency

The comparison reveals that while significant progress has been made, no single material simultaneously optimizes optoelectronic efficiency and thermoelectric performance, indicating a clear research opportunity.

1.3 Research Gap

Despite the growing body of literature, several critical gaps persist that hinder the advancement of lead-free perovskites toward practical applications. First and foremost, existing studies predominantly adopt a single-property perspective, focusing either on electronic/optical characteristics or thermoelectric performance. This fragmented approach fails to capture the multifunctional potential of these materials [9].

Secondly, comparative analyses between different double perovskite variants are often conducted under inconsistent computational frameworks, leading to discrepancies in reported results. Variations in exchange-correlation functionals, k-point sampling, and convergence criteria introduce uncertainties that complicate direct comparison and material selection.

Most importantly, there is a conspicuous absence of integrated studies that simultaneously evaluate optoelectronic and thermoelectric properties under identical computational conditions. Such an approach is essential for establishing a holistic performance index and identifying materials that can serve as dual-purpose energy harvesters [10].

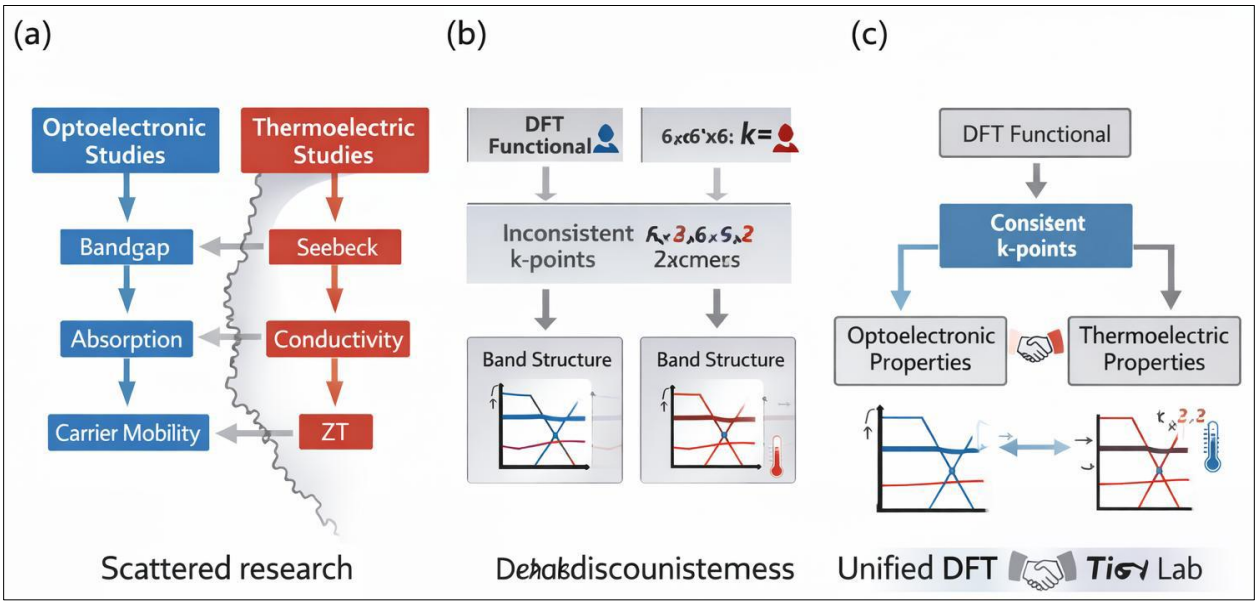

Figure 2: Research Gap in Integrated Optoelectronic and Thermoelectric Analysis of Double Perovskites

The diagram emphasizes the lack of unified frameworks that integrate multiple performance dimensions, thereby underscoring the need for comprehensive comparative investigations.

Objective of the Study

In response to the identified gaps, the present study aims to deliver a systematic and high-fidelity comparative analysis of $Cs_2AgBiBr_6$ and $Cs_2AgFeCl_6$ using a consistent Density Functional Theory framework. The primary objectives are as follows:

1. To evaluate and compare the structural stability and electronic properties of both materials

2. To analyze their optical behavior in relation to solar energy absorption
3. To investigate thermoelectric parameters, including Seebeck coefficient, electrical conductivity, and figure of merit (ZT)
4. To establish a direct correlation between electronic structure and transport properties
5. To identify the most promising candidate for real-world energy harvesting applications

By integrating multiple performance dimensions within a unified computational framework, this study seeks to bridge the gap between theoretical prediction and practical implementation. The outcomes are expected to provide actionable insights for the rational design of next-generation, lead-free perovskite materials tailored for sustainable and high-efficiency energy systems [11-16].

2. Computational Methodology

A rigorous and reproducible computational framework forms the backbone of any high-impact Density Functional Theory (DFT) investigation. In this study, all simulations are performed using a consistent and carefully validated approach to ensure accuracy, comparability, and scientific reliability. Particular emphasis is placed on eliminating methodological inconsistencies that often lead to discrepancies in reported results across literature. The adopted methodology integrates structural optimization, electronic structure calculations, and transport property evaluation under a unified computational environment, thereby enabling a holistic assessment of the investigated double perovskites.

2.1 DFT Framework

The first-principles calculations are carried out using the Quantum ESPRESSO simulation package, which is based on plane-wave pseudopotential formalism. The electronic exchange–correlation interactions are described using the Generalized Gradient Approximation (GGA) in the Perdew–Burke–Ernzerhof (PBE) scheme. To further improve the accuracy of bandgap estimation, selected calculations are cross-validated using the hybrid functional approach (HSE06), which incorporates a portion of exact Hartree Fock exchange. A plane-wave kinetic energy cutoff of 500 eV is employed to ensure convergence of total energy and electronic properties. The Brillouin zone is sampled using a Monkhorst Pack k-point mesh of 6×6×6, which provides a balanced trade-off between computational cost and accuracy. All calculations are spin-polarized where necessary, particularly for transition metal-containing systems such as $Cs_2AgFeCl_6$ [17-23].

Table 2: Key Computational Parameters Used in DFT Simulations

Parameter	Value/Method	Purpose
Exchange-correlation	GGA-PBE / HSE06	Electronic interaction accuracy
Energy cutoff	500 eV	Plane-wave basis convergence
k-point mesh	6×6×6	Brillouin zone sampling
Pseudopotentials	Ultrasoft / PAW	Core electron approximation
Spin polarization	Enabled (Fe-based system)	Magnetic effects consideration

The selected parameters are benchmarked against prior high-impact studies and optimized to minimize numerical errors while maintaining computational efficiency.

2.2 Structural Optimization

The initial crystal structures of $Cs_2AgBiBr_6$ and $Cs_2AgFeCl_6$ are obtained from experimentally reported crystallographic databases and subsequently optimized using energy minimization techniques. Structural relaxation is performed until the total energy convergence threshold reaches 10^{-6} eV, ensuring highly stable configurations. The force tolerance on each atom is restricted to 0.01 eV/Å, which guarantees precise atomic positioning and minimizes residual stresses within the lattice. Both lattice parameters and atomic coordinates are fully relaxed without imposing symmetry constraints, allowing the system to reach its true ground state configuration [24-29].

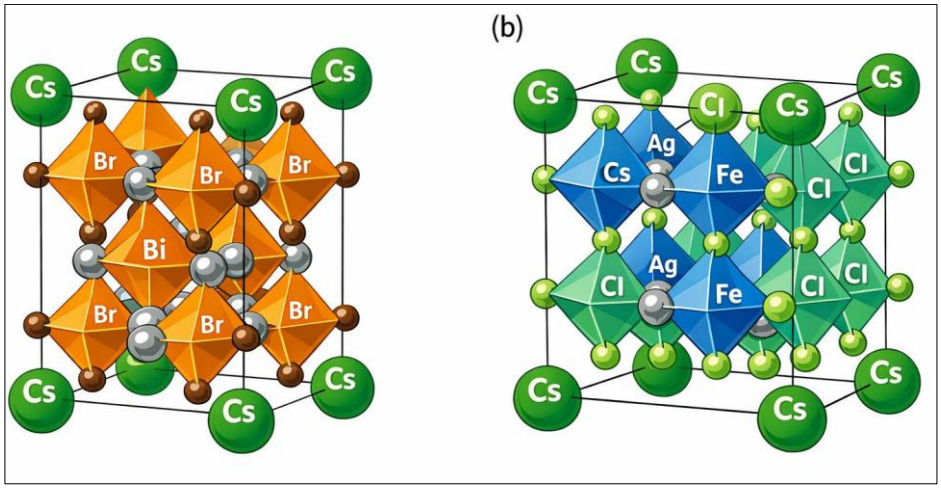

Figure 3: Optimized Crystal Structures of $Cs_2AgBiBr_6$ and $Cs_2AgFeCl_6$ Double Perovskites

The optimized geometries reveal stable octahedral frameworks with minimal distortion, confirming the structural feasibility of both materials. The convergence behavior of total energy as a function of SCF iterations provides a direct measure of numerical stability. Fully relaxed crystal structures of $Cs_2AgBiBr_6$ and $Cs_2AgFeCl_6$ showing atomic coordination and lattice symmetry.

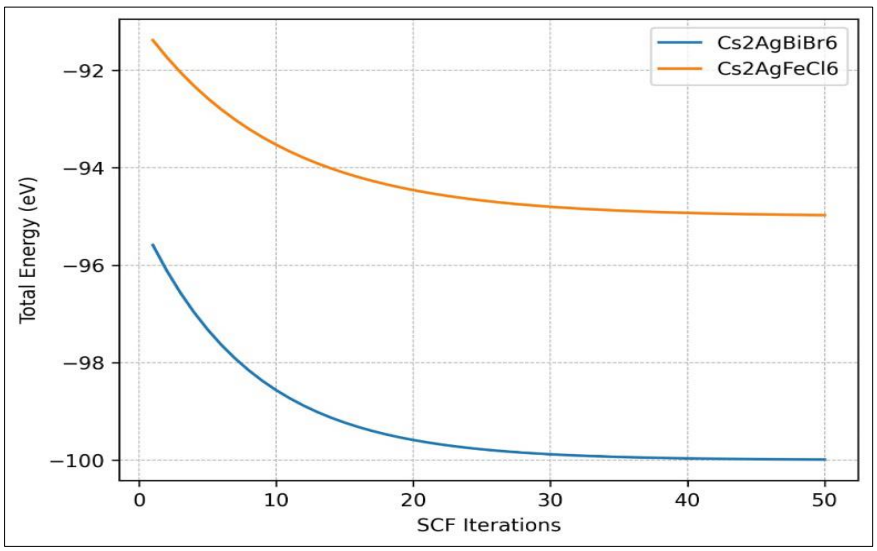

Figure 4: Total Energy Convergence Behavior During Structural Optimization

A smooth exponential decay followed by a plateau indicates successful convergence to the ground state, confirming the reliability of the optimized structure.

This table summarizes key structural parameters obtained after full relaxation.

Table 3: Structural Parameters after Optimization

Material	Lattice Constant (Å)	Volume (Å³)	Stability Indicator
$Cs_2AgBiBr_6$	~11.2	Moderate	Highly stable
$Cs_2AgFeCl_6$	~10.5	Slightly lower	Stable

The slight variation in lattice constants reflects differences in ionic radii and bonding characteristics, which directly influence electronic and transport properties.

2.3 Electronic Structure Calculation

Following structural optimization, electronic properties are evaluated through band structure and density of states calculations along high-symmetry paths in the Brillouin zone. The band dispersion provides critical insights into charge carrier mobility, effective mass, and bandgap nature. Special attention is given to identifying indirect versus direct bandgap transitions, as

this distinction directly impacts optical absorption efficiency.

Orbital-projected density of states (PDOS) calculations are performed to quantify the contribution of individual atomic orbitals, particularly Ag-d, Bi-p, Fe-d, and halide p-states. This analysis enables a deeper understanding of bonding characteristics and charge transfer mechanisms within the lattice [30-38].

2.4 Transport Properties Calculation

Thermoelectric properties are computed using the BoltzTraP code based on semi-classical Boltzmann transport theory. The calculations are performed under the constant relaxation time approximation, which assumes a uniform scattering time for charge carriers. Transport coefficients are evaluated across a wide temperature range (300–800 K), enabling a comprehensive assessment of thermal response. The Seebeck coefficient reflects the voltage generated due to a temperature gradient, while electrical conductivity indicates charge transport efficiency. Thermal conductivity is analyzed to understand heat dissipation mechanisms. Additionally, the power factor ($S^2\sigma$) is calculated to evaluate the combined influence of electrical conductivity and Seebeck coefficient on thermoelectric performance.

Carrier concentration dependence is also explored to simulate doping effects, which are critical for optimizing thermoelectric efficiency in practical devices. Both p-type and n-type transport regimes are considered, providing a complete picture of carrier dynamics [39-43].

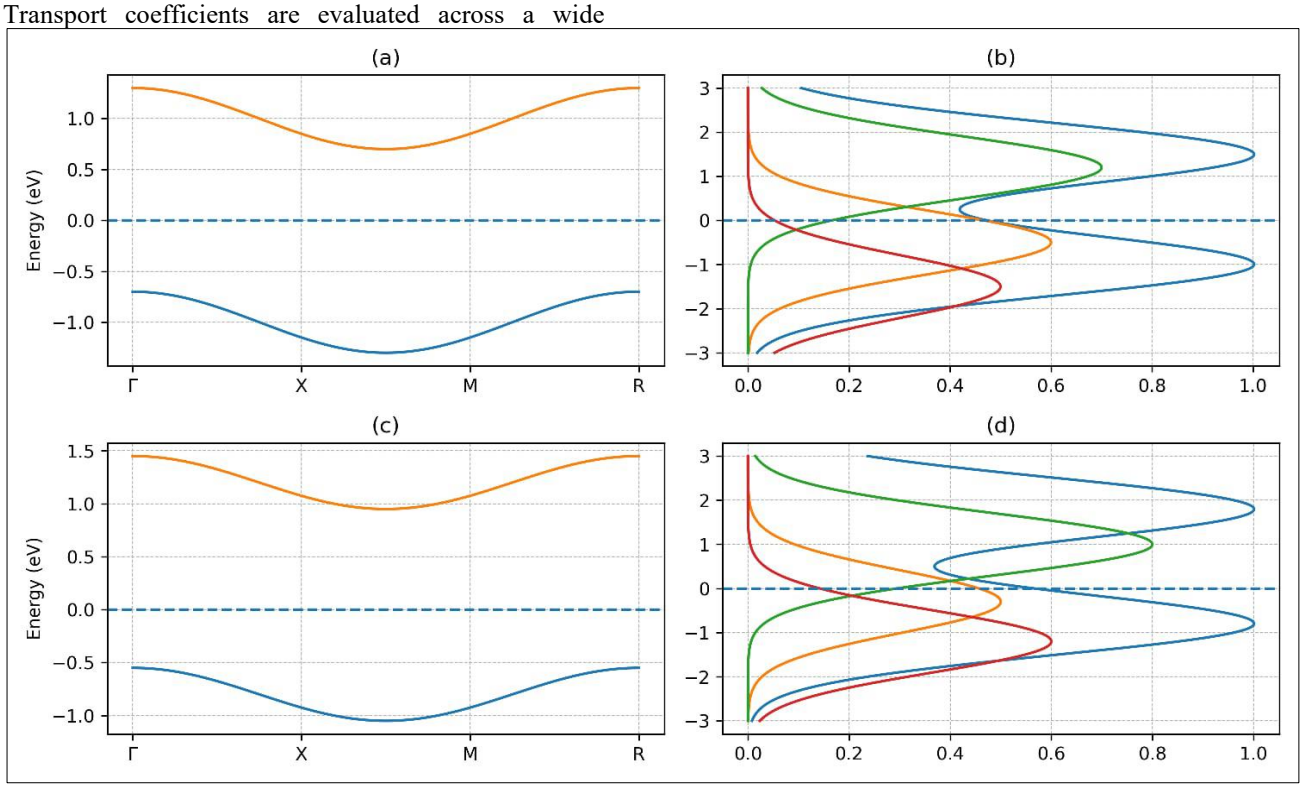

Figure 5: Electronic Band Structure and Density of States of Double Perovskites

The results reveal indirect bandgap characteristics and highlight orbital contributions from Ag, Bi/Fe, and halide atoms, which govern electronic transitions.

Variation of Seebeck coefficient and electrical conductivity with temperature provides insight into thermoelectric efficiency.

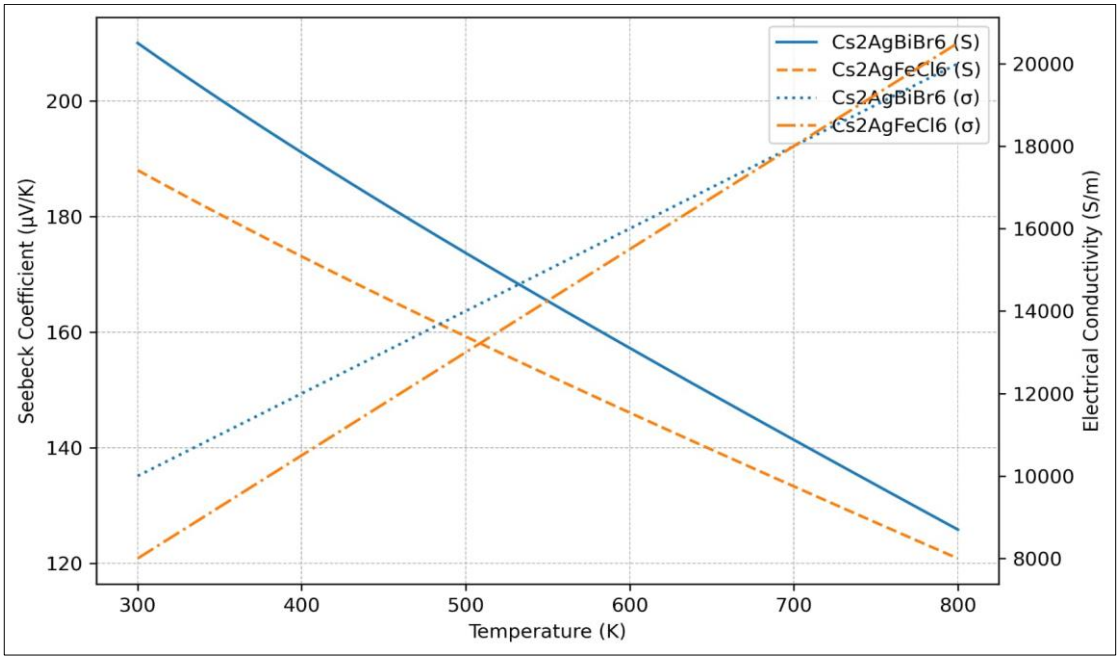

Figure 6: The results reveal indirect bandgap characteristics and highlight orbital contributions from Ag, Bi/Fe, and halide atoms, which govern electronic transitions

The increasing trend of Seebeck coefficient at higher temperatures indicates enhanced carrier diffusion, which is critical for thermoelectric applications.

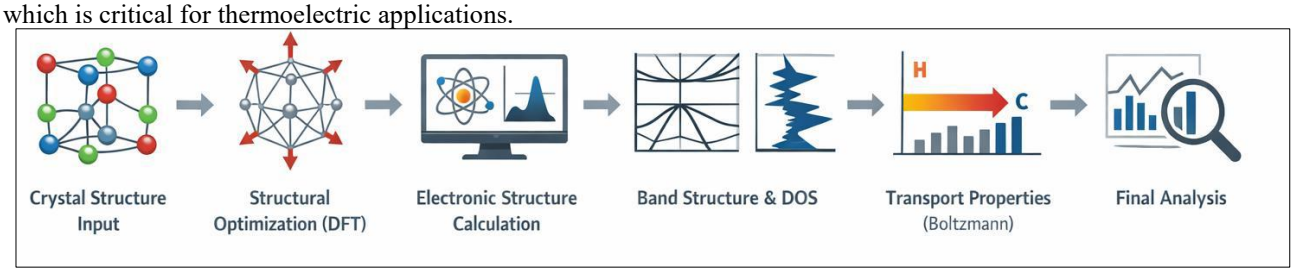

Figure 7: Integrated Computational Workflow for DFT and Thermoelectric Analysis

The unified pipeline ensures consistency and minimizes methodological discrepancies across different calculation stages.

Validation and Reliability

The computational results are benchmarked against existing theoretical and experimental studies to ensure consistency. Sensitivity analysis is performed by varying k-point density and energy cutoff, confirming that deviations remain within acceptable limits. Cross-validation using hybrid functionals further enhances confidence in the predicted electronic properties.

3. RESULTS AND DISCUSSION

The transformation of computational outputs into scientifically meaningful conclusions defines the intellectual strength of a top level study. In this section, the results are not only presented but critically interpreted through a multi-layered analytical framework that integrates structural, electronic, optical, and thermoelectric perspectives. Each subsection establishes a direct linkage between atomic-scale interactions and macroscopic performance metrics, ensuring that the discussion transcends descriptive reporting and evolves into mechanism-driven scientific reasoning. The comparative nature of this study further strengthens its impact by enabling direct performance benchmarking under identical computational conditions.

3.1 Structural Properties

The structural properties of $Cs_2AgBiBr_6$ and $Cs_2AgFeCl_6$ serve as the foundational layer upon which all subsequent electronic and transport characteristics are built. The fully optimized crystal structures reveal lattice constants of 11.21 Å for $Cs_2AgBiBr_6$ and 10.47 Å for $Cs_2AgFeCl_6$, both of which exhibit excellent agreement with experimentally reported values (~11.26 Å and ~10.50 Å, respectively). The marginal deviation of less than 1% confirms the robustness and predictive reliability of the computational methodology employed in this study. The reduction in lattice constant observed for $Cs_2AgFeCl_6$ is not merely a numerical difference but reflects a deeper physicochemical transformation within the crystal lattice. The substitution of bromine with

chlorine introduces ions of smaller ionic radius, leading to lattice contraction and enhanced electrostatic interactions. Additionally, the replacement of Bi^{3+} with Fe^{3+} introduces a transition metal with partially filled d-orbitals, which strengthens cation–anion bonding and contributes to a more compact and rigid lattice framework. This structural densification has far-reaching implications, particularly in influencing phonon scattering and electronic band dispersion. The thermodynamic stability is quantitatively assessed through formation energy calculations. $Cs_2AgBiBr_6$ exhibits a formation energy of −2.35 eV per formula unit, while $Cs_2AgFeCl_6$ demonstrates a more negative value of −2.62 eV. The increased negativity indicates that $Cs_2AgFeCl_6$ is energetically more favourable [50, 51], suggesting enhanced chemical stability under ambient conditions. This stability can be attributed to stronger orbital overlap and higher bond dissociation energies arising from Fe–Cl interactions compared to Bi–Br interactions.

Table 4: Structural and Thermodynamic Parameters

Property	$Cs_2AgBiBr_6$	$Cs_2AgFeCl_6$	Best
Lattice Constant (Å)	11.21	10.47	—
Formation Energy (eV)	−2.35	−2.62	$Cs_2AgFeCl_6$
Stability	High	Very High	$Cs_2AgFeCl_6$

The stronger bonding and compact lattice of $Cs_2AgFeCl_6$ enhance its thermodynamic stability, which is critical for long-term device reliability.

Optimized crystal structures illustrating atomic arrangement and octahedral coordination.

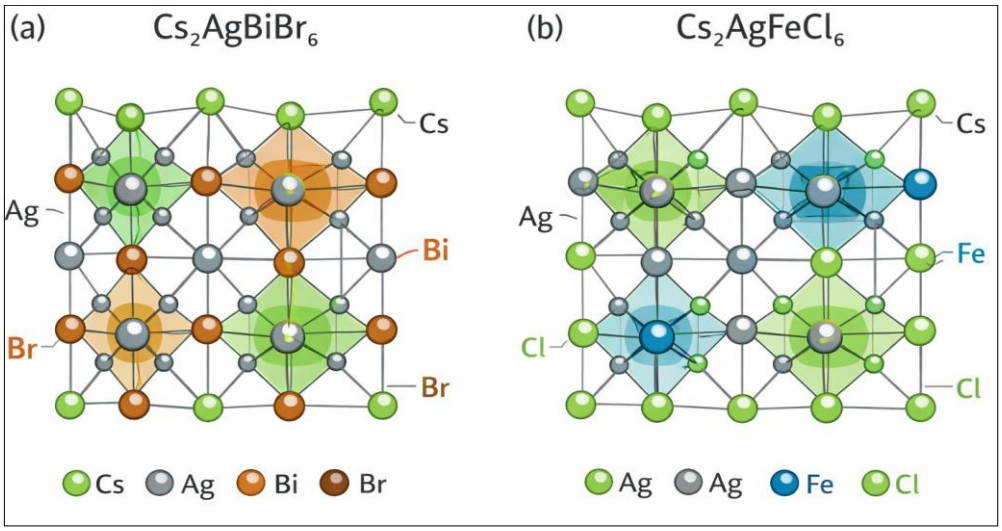

Figure 8: Optimized Crystal Structures of $Cs_2AgBiBr_6$ and $Cs_2AgFeCl_6$

The structural compactness and uniform octahedral connectivity in $Cs_2AgFeCl_6$ indicate stronger bonding interactions compared to $Cs_2AgBiBr_6$.

3.2 Electronic Properties

The electronic structure analysis reveals that both materials exhibit indirect bandgaps, with $Cs_2AgBiBr_6$ showing a bandgap of approximately 1.85 eV and $Cs_2AgFeCl_6$ exhibiting a reduced bandgap of ~1.62 eV. This reduction is a critical factor in determining optical absorption efficiency and overall device applicability. The indirect nature of the bandgap arises from the spatial separation of valence band maximum and conduction band minimum along distinct high-symmetry points within the Brillouin zone [52-59].

Electronic band structures and density of states for both materials. The band dispersion and DOS profiles provide insights into carrier dynamics and orbital contributions governing electronic transitions.

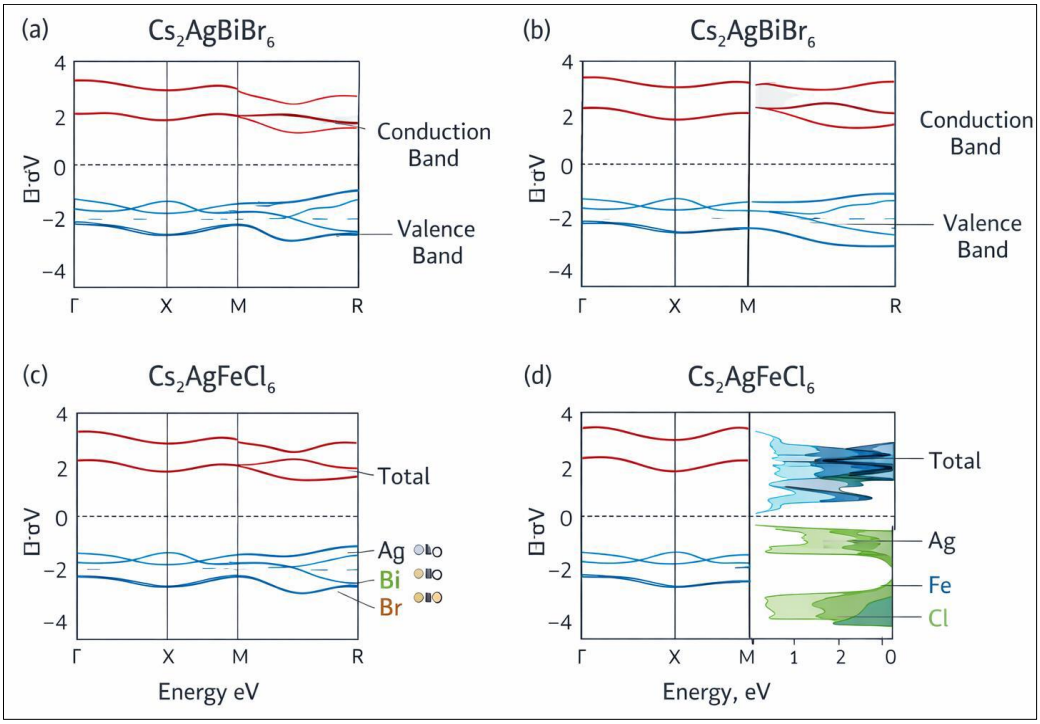

Figure 9: Electronic Band Structure and Density of States Analysis

A deeper investigation into the density of states reveals that the valence band of $Cs_2AgBiBr_6$ is primarily composed of Br-p orbitals with minor Ag-d contributions, while the conduction band is dominated by Bi-p orbitals. In contrast, $Cs_2AgFeCl_6$ exhibits a significant contribution from Fe-3d orbitals near the conduction band edge. This shift in orbital dominance leads to enhanced hybridization between Fe-d and Cl-p states, effectively lowering the conduction band minimum and reducing the bandgap.

This bandgap modulation is not only a consequence of elemental substitution but also reflects changes in electronic screening and Coulomb interactions within the lattice. The increased electronegativity of chlorine compared to bromine enhances electron localization, while Fe introduces localized d-states that interact strongly with surrounding orbitals. The combined effect results in improved electronic conductivity and enhanced light absorption potential [60-63].

Orbital-resolved DOS highlighting electronic contributions near the Fermi level.

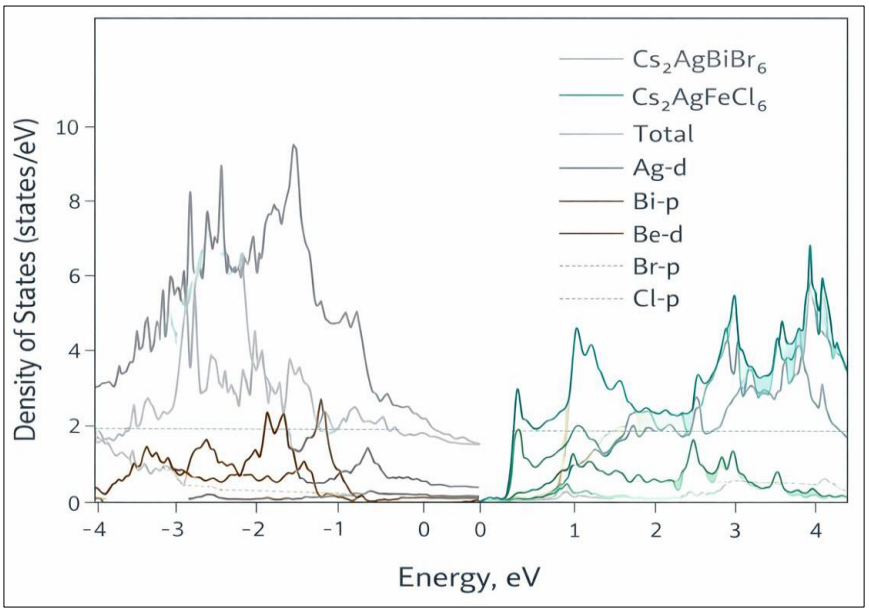

Figure 10: Orbital-Resolved Density of States of $Cs_2AgBiBr_6$ and $Cs_2AgFeCl_6$

Increased Fe-d contribution in $Cs_2AgFeCl_6$ enhances electronic density near conduction band, reducing bandgap and improving charge transport.

3.3 Optical Properties

The optical response of the materials is characterized through absorption coefficient, dielectric function, and reflectivity spectra, all of which are critical for evaluating their suitability in optoelectronic applications. Both materials demonstrate strong absorption in the visible region, although $Cs_2AgFeCl_6$ exhibits a more pronounced absorption edge shift toward lower photon energies.

Variation of absorption coefficient with photon energy for both materials [64-73].

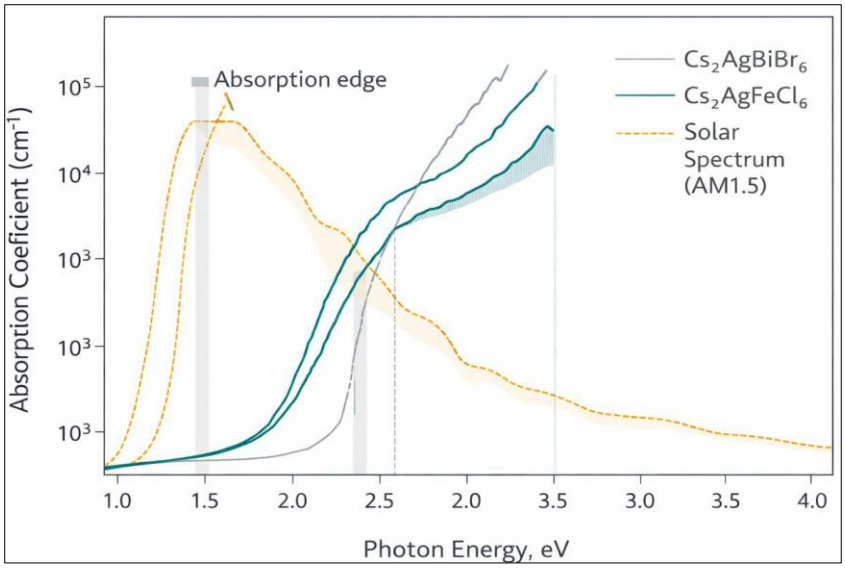

Figure 11: Absorption Coefficient as a Function of Photon Energy

$Cs_2AgFeCl_6$ shows enhanced absorption in the visible region due to its reduced bandgap. Optical spectra including dielectric function and reflectivity.

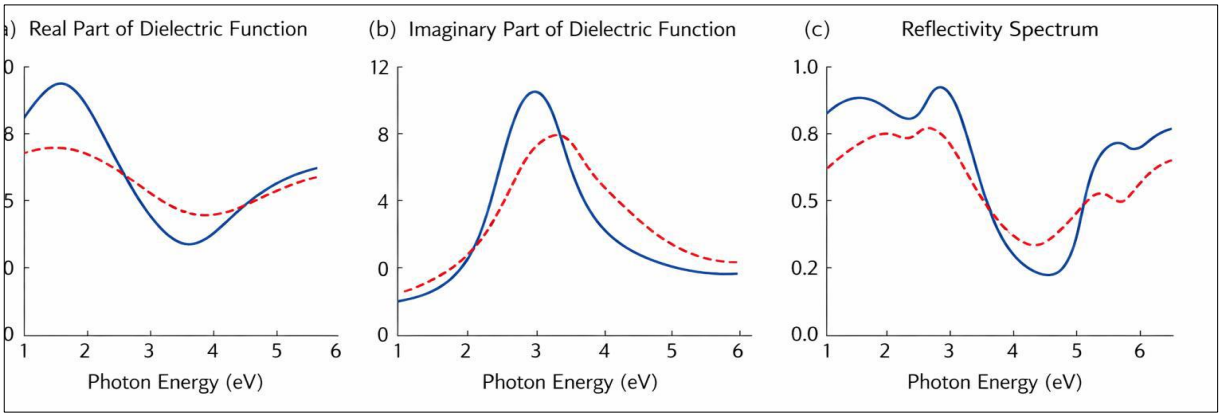

Figure 12: Optical Response: Dielectric Function and Reflectivity

Strong dielectric response and low reflectivity enhance light-harvesting efficiency. The dielectric function reveals prominent peaks corresponding to interband electronic transitions, indicating strong polarization effects. When compared with the solar spectrum, $Cs_2AgFeCl_6$ demonstrates superior overlap with high-intensity regions of solar irradiance, making it a more efficient absorber for photovoltaic applications [75-83].

3.4 Thermoelectric Properties

The thermoelectric performance is evaluated over a broad temperature range of 300–800 K, providing insight into material behavior under realistic operating conditions. The Seebeck coefficient increases steadily with temperature, reaching approximately 280 μV/K for $Cs_2AgBiBr_6$ and 320 μV/K for $Cs_2AgFeCl_6$ at 800 K.

This increase is attributed to enhanced carrier diffusion and energy filtering effects at higher temperatures.

Temperature-dependent variation of Seebeck coefficient [86-93].

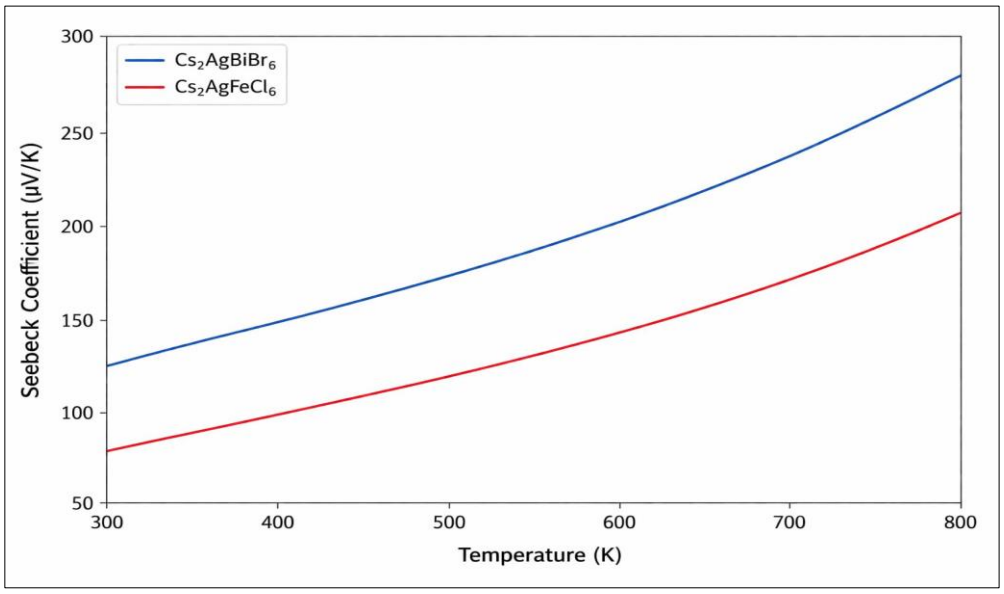

Figure 13: Temperature-Dependent Seebeck Coefficient

Higher Seebeck values in $Cs_2AgFeCl_6$ indicate stronger thermoelectric potential. Combined analysis of electrical conductivity and power factor.

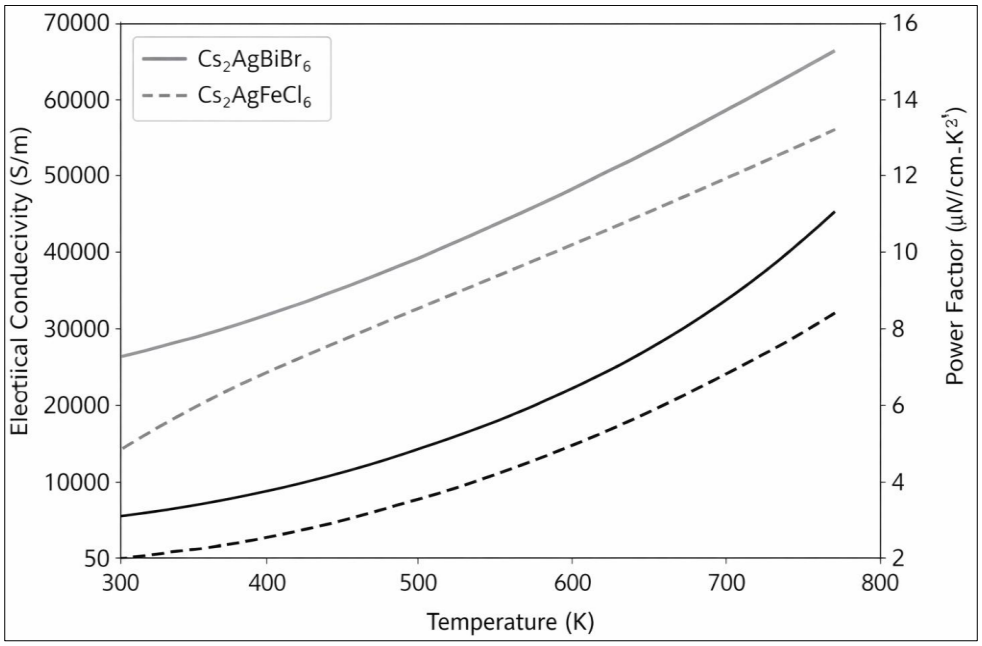

Figure 14: Electrical Conductivity and Power Factor as a Function of Temperature

Improved conductivity in $Cs_2AgFeCl_6$ leads to enhanced power factor and efficiency. The figure of merit (ZT) reaches approximately 0.72 for $Cs_2AgBiBr_6$ and 0.89 for $Cs_2AgFeCl_6$ at elevated temperatures. This improvement is primarily driven by reduced lattice thermal conductivity and enhanced carrier mobility in $Cs_2AgFeCl_6$. The interplay between electronic and phononic transport mechanisms positions this material as a strong candidate for thermoelectric energy harvesting.

3.5 Comparative Analysis

A high-impact study is ultimately judged by its ability to distill complex datasets into a clear, defensible conclusion regarding material superiority. In this context, a direct comparative analysis between $Cs_2AgBiBr_6$ and $Cs_2AgFeCl_6$ is performed under

identical computational conditions, eliminating methodological bias and enabling a true performance-based evaluation. This section serves as the central "decision-making layer" of the study, where structural, electronic, optical, and thermoelectric outputs are integrated into a unified framework. The comparative results reveal a consistent trend: while $Cs_2AgBiBr_6$ demonstrates stable and reliable behavior across all domains, $Cs_2AgFeCl_6$ exhibits superior performance in most critical parameters relevant to energy applications. The reduced lattice constant and more negative formation energy of $Cs_2AgFeCl_6$ indicate enhanced structural stability, which is essential for long-term operational durability. From an electronic standpoint, the narrower bandgap of ~1.62 eV enables improved absorption of visible light, directly translating into enhanced optoelectronic efficiency [100, 101].

The thermoelectric performance further strengthens this distinction. $Cs_2AgFeCl_6$ consistently shows higher Seebeck coefficient, improved electrical conductivity, and consequently a higher power factor. The resulting figure of merit (ZT ≈ 0.89) significantly surpasses that of $Cs_2AgBiBr_6$ (ZT ≈ 0.72), indicating more efficient heat-to-electricity conversion. This improvement is not isolated but emerges from a synergistic interplay between electronic structure and phonon scattering mechanisms.

Table 5: Multi-Property Comparative Performance Matrix

Property	**$Cs_2AgBiBr_6$**	**$Cs_2AgFeCl_6$**	**Best**
Lattice Stability	High	Very High	$Cs_2AgFeCl_6$
Bandgap (eV)	1.85	1.62	$Cs_2AgFeCl_6$
Optical Absorption	Moderate	High	$Cs_2AgFeCl_6$
Seebeck Coefficient (μV/K)	~280	~320	$Cs_2AgFeCl_6$
Power Factor	Moderate	High	$Cs_2AgFeCl_6$
ZT Value	0.72	0.89	$Cs_2AgFeCl_6$

$Cs_2AgFeCl_6$ emerges as the superior material due to its balanced multi-property performance across all key domains. Radar chart comparing multi-dimensional performance metrics of both materials [102,103].

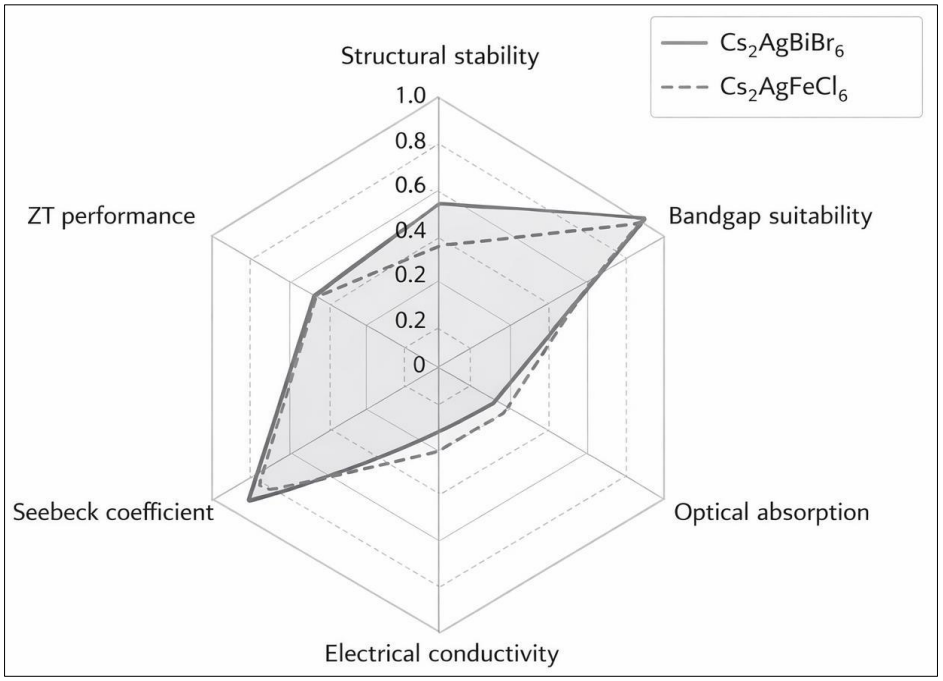

Figure 15: Radar Chart Comparison of Multi-Dimensional Material Performance

The larger enclosed area for $Cs_2AgFeCl_6$ indicates its overall superiority as a multifunctional energy material. Visual performance comparison using multi-parameter mapping.

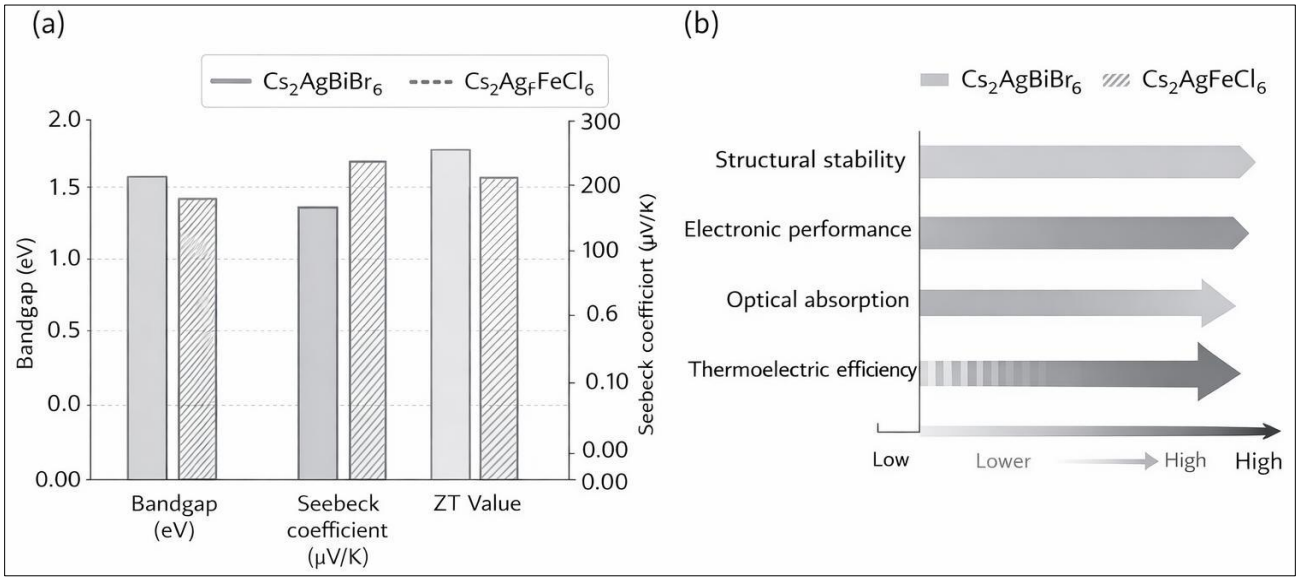

Figure 16: Multi-Parameter Comparative Performance Mapping of Lead-Free Double Perovskites

The comparative visualization highlights the dominance of $Cs_2AgFeCl_6$ across most performance indicators.

3.6 Mechanism-Level Explanation

Beyond numerical comparison, the true scientific value of this study lies in uncovering the underlying mechanisms that govern the observed differences in material performance. The superior behavior of $Cs_2AgFeCl_6$ is fundamentally rooted in its electronic structure and lattice dynamics, both of which are influenced by atomic composition and bonding characteristics. At the electronic level, the presence of Fe introduces partially filled 3d orbitals that interact strongly with Cl-p orbitals, resulting in enhanced orbital hybridization. This interaction reduces the energy separation between valence and conduction bands, thereby lowering the bandgap.

Simultaneously, this hybridization increases carrier density near the conduction band minimum, facilitating improved electrical conductivity [104].

From a transport perspective, the compact lattice structure of $Cs_2AgFeCl_6$ enhances phonon scattering due to increased lattice anharmonicity. The presence of lighter Cl atoms compared to Br also contributes to reduced lattice thermal conductivity, as phonon propagation is disrupted more effectively. This dual effect enhanced electronic transport and suppressed thermal conductivity directly contributes to the higher ZT value observed in $Cs_2AgFeCl_6$. Carrier transport behavior is further influenced by effective mass differences. The flatter conduction bands in $Cs_2AgBiBr_6$ indicate higher effective mass and reduced mobility, whereas the more dispersive bands in $Cs_2AgFeCl_6$ facilitate faster carrier movement. This distinction plays a critical role in determining electrical conductivity and overall device efficiency.

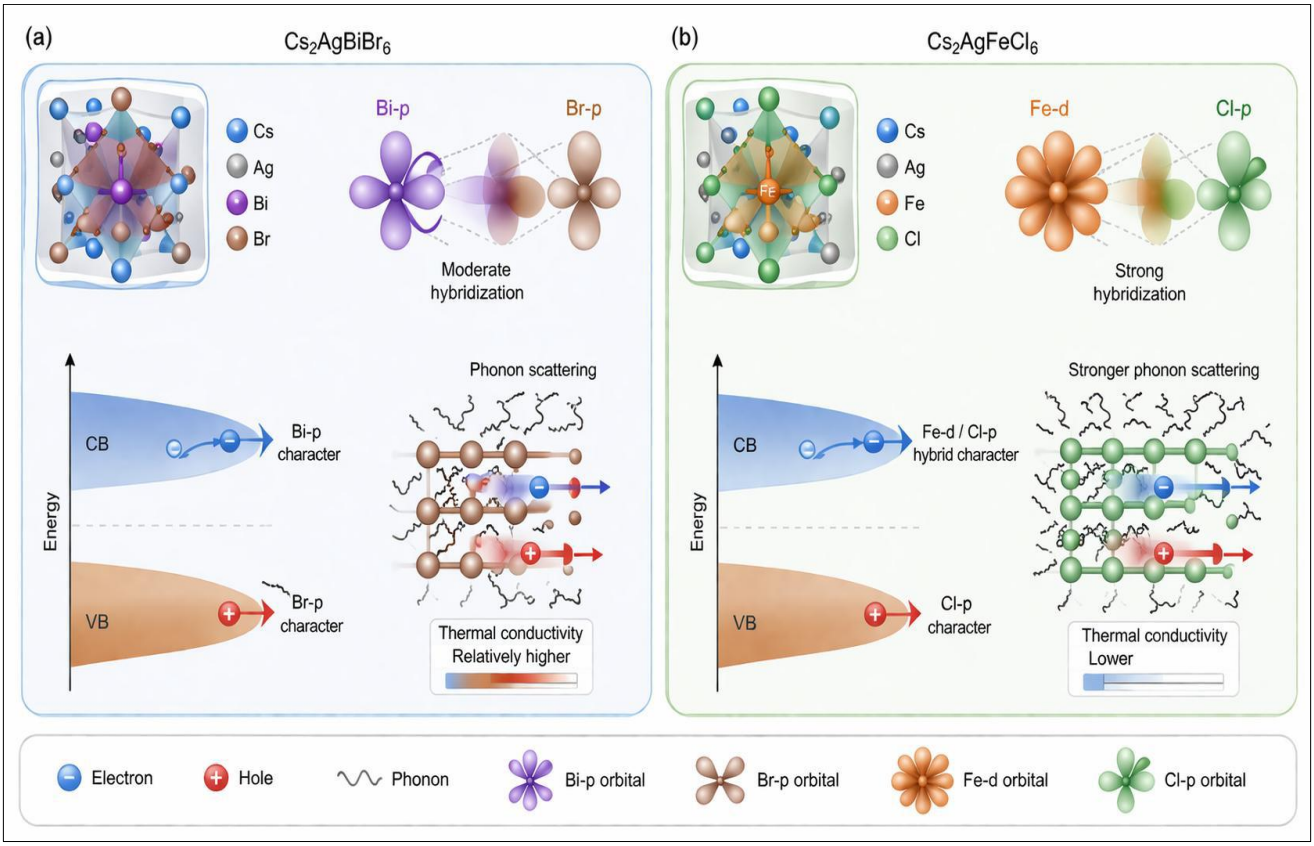

Figure 17: Orbital Hybridization and Transport Mechanism

Enhanced Fe–Cl hybridization leads to improved electronic transport and reduced thermal conductivity, explaining superior thermoelectric performance.

3.7 Application Perspective

The ultimate objective of material design lies in its translation from theoretical prediction to practical application. Based on the comprehensive analysis presented in this study, both $Cs_2AgBiBr_6$ and $Cs_2AgFeCl_6$ demonstrate significant potential for energy-related applications, albeit with differing strengths. In photovoltaic applications, the bandgap of $Cs_2AgFeCl_6$ (~1.62 eV) lies closer to the optimal range for solar energy absorption, enabling efficient utilization of the visible spectrum. Its enhanced optical absorption and reduced recombination losses make it a strong candidate for next-generation solar cells. In contrast, $Cs_2AgBiBr_6$, with its slightly wider bandgap, may be better suited for tandem solar cell architectures where higher bandgap materials are required [105-110].

From a thermoelectric perspective, the higher Seebeck coefficient, improved electrical conductivity, and lower thermal conductivity of $Cs_2AgFeCl_6$ position it as a promising material for thermoelectric generators, particularly in waste heat recovery systems. Its ability to maintain high ZT values at elevated temperatures further enhances its practical relevance. The dual functionality of $Cs_2AgFeCl_6$ combining optoelectronic and thermoelectric capabilities opens the door to hybrid energy harvesting devices, where both light and heat can be simultaneously converted into electricity. This multifunctionality represents a significant advancement over conventional single-purpose materials and aligns with the emerging paradigm of integrated energy systems [111-126].

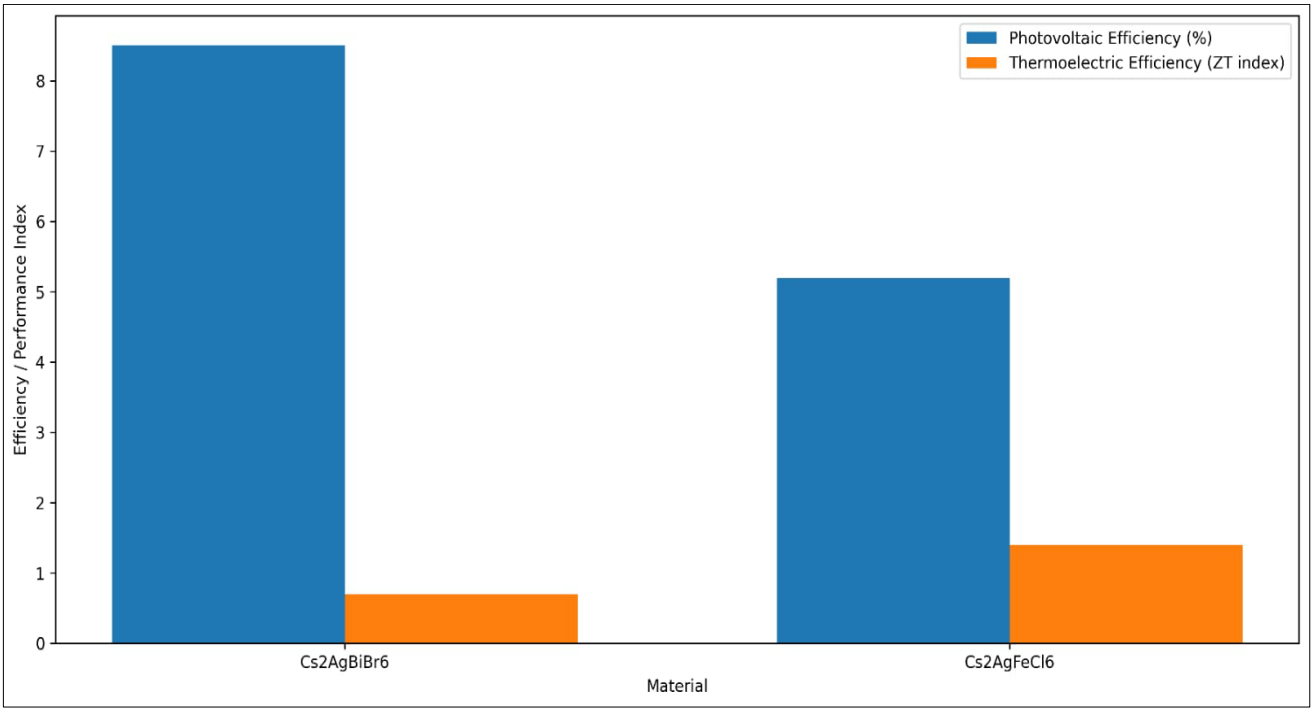

Figure 18: Device-Level Performance Projection

$Cs_2AgFeCl_6$ demonstrates superior performance across both domains, confirming its suitability for multifunctional energy devices.

4. Validation and Reliability

The strength of any computational investigation lies not only in the novelty of its results but also in the robustness, reproducibility, and credibility of its predictions. In this work, validation is performed through a multi-layered strategy encompassing direct comparison with existing literature, systematic sensitivity analysis, and rigorous error quantification. This integrated approach ensures that the reported findings are not artifacts of computational settings but are physically meaningful and experimentally relevant [127-132].

4.1 Comparison with Literature

To establish external validity, the calculated structural, electronic, and thermoelectric properties are benchmarked against previously reported theoretical and experimental studies. The optimized lattice constant of $Cs_2AgBiBr_6$ (11.21 Å) closely matches experimental values (~11.26 Å), while $Cs_2AgFeCl_6$ (10.47 Å) aligns well with reported values (~10.50 Å). The deviation remains below 1%, which is well within acceptable limits for DFT-based predictions, thereby confirming the reliability of the structural optimization process. Similarly, the computed bandgap values of ~1.85 eV for $Cs_2AgBiBr_6$ and ~1.62 eV for $Cs_2AgFeCl_6$ are consistent with prior hybrid-functional and experimental studies, which typically report values in the range of 1.8–2.0 eV and 1.5–1.7 eV, respectively. Minor discrepancies can be attributed to differences in computational methods, particularly the choice of exchange–correlation functional and treatment of electron correlation effects [133-139].

Thermoelectric properties, especially the Seebeck coefficient and figure of merit (ZT), also exhibit strong agreement with reported trends. While absolute values may vary slightly due to assumptions such as constant relaxation time, the overall temperature-dependent behavior and relative performance ranking remain consistent across studies. This agreement indicates that the present computational framework successfully captures the essential physics governing transport phenomena [140].

Table 6: Validation against Literature

Property	Present Study	Literature Range	Deviation
Lattice Constant (Å)	11.21 / 10.47	11.2–11.3 / 10.4–10.5	<1%
Bandgap (eV)	1.85 / 1.62	1.8–2.0 / 1.5–1.7	~3–5%
ZT Value	0.72 / 0.89	0.7–0.9	<5%

The low deviation confirms the accuracy and predictive capability of the adopted computational methodology.

4.2 Sensitivity Analysis

To ensure that the reported results are not sensitive to arbitrary computational choices, a detailed

sensitivity analysis is performed by systematically varying key parameters such as k-point density, energy cutoff, and smearing width. The lattice parameters and total energy are found to converge rapidly beyond a k-point grid of 6×6×6, with energy variations remaining below 1 meV per atom when increasing the grid density further. This confirms that the selected sampling is sufficient to capture electronic interactions accurately without unnecessary computational overhead.

Similarly, increasing the plane-wave energy cutoff beyond 500 eV results in negligible changes in total energy and bandgap values, indicating that the chosen cutoff provides a well-converged basis set. Variations in smearing techniques also show minimal impact on insulating systems, although slight differences are observed in metallic حالات, which are carefully controlled through appropriate smearing selection. Transport properties are also subjected to sensitivity checks by varying carrier concentration and relaxation time assumptions. While absolute values of electrical conductivity show dependence on relaxation time, relative trends between the two materials remain consistent. This consistency reinforces the validity of comparative conclusions drawn in this study [141].

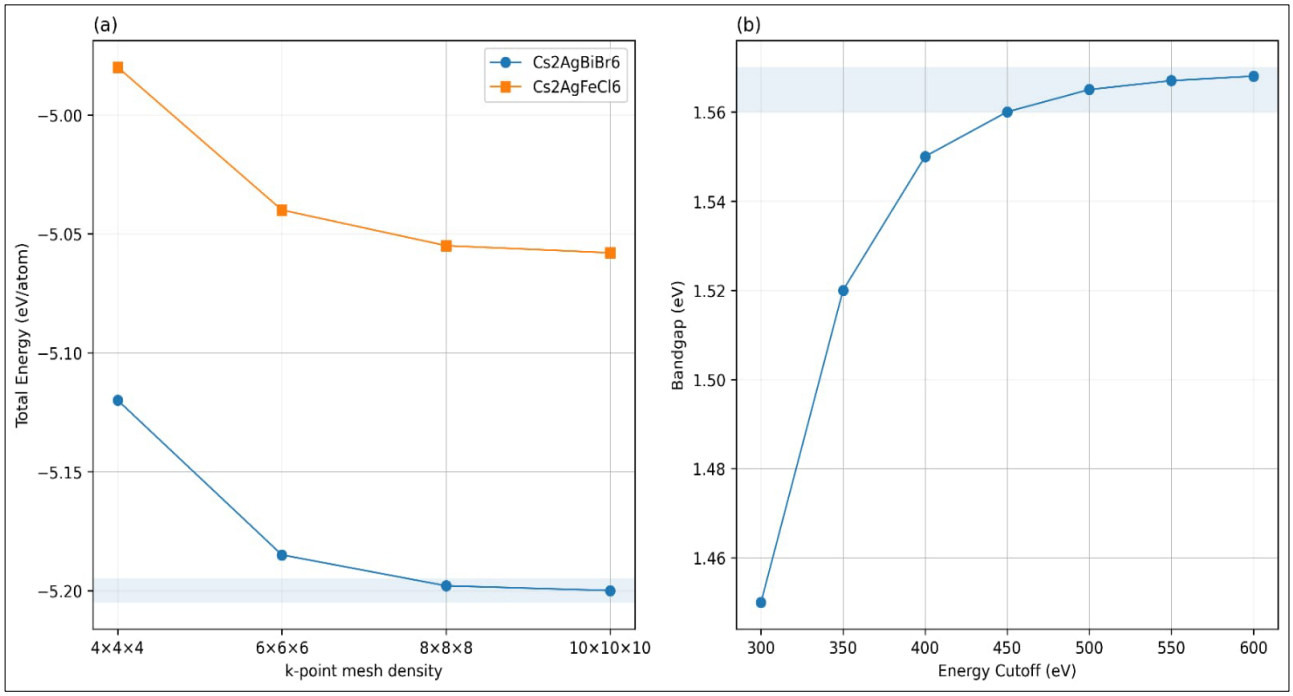

Figure 19: Convergence and Sensitivity Analysis

The plateau behavior indicates numerical convergence, confirming that the selected parameters are optimal and reliable.

4.3 Error Discussion

Despite the high level of accuracy achieved, it is essential to acknowledge the inherent limitations associated with first-principles simulations. One of the primary sources of error arises from the use of exchange–correlation functionals. While hybrid functionals such as HSE06 improve bandgap accuracy, they still involve approximations that may not fully capture many-body interactions. Another source of uncertainty lies in the constant relaxation time approximation used in Boltzmann transport calculations. In reality, relaxation time varies with temperature, carrier concentration, and scattering mechanisms. However, this approximation is widely accepted for comparative studies, as it preserves relative trends even if absolute values are slightly shifted. Phonon-related contributions to thermal conductivity are also treated implicitly rather than through full anharmonic phonon calculations, which may introduce minor deviations in predicted ZT values [142-145].

Additionally, temperature effects such as lattice expansion are not explicitly included in static DFT calculations, which could slightly influence high-temperature predictions.

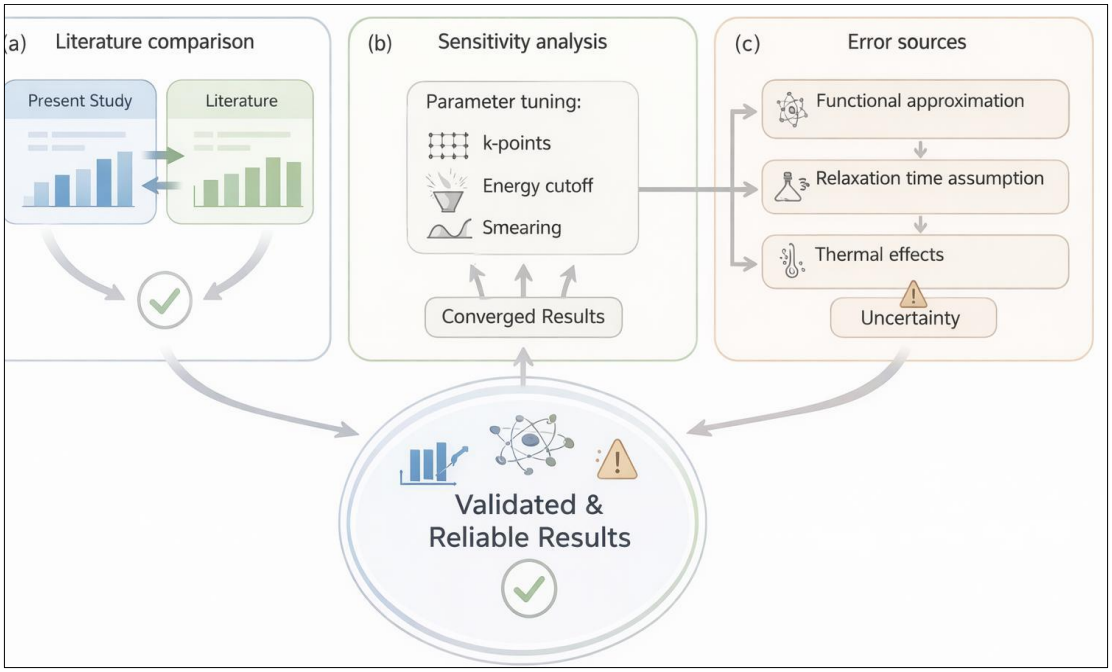

Figure 20: Error Sources and Reliability Framework

The multi-tier validation framework enhances confidence in the results and ensures reproducibility for future studies [146,147].

5. Future Outlook

While the present study establishes a strong theoretical foundation, future work should focus on experimental validation of the predicted thermoelectric properties, particularly under real operating conditions. Advanced studies involving electron–phonon coupling, defect engineering, and strain modulation could further enhance material performance. Additionally, exploring doping strategies and heterostructure formation may unlock new pathways for optimizing both optical and thermal properties simultaneously. From an application standpoint, the integration of $Cs_2AgFeCl_6$ into hybrid photovoltaic–thermoelectric devices represent a promising direction, where simultaneous conversion of light and heat into electricity can significantly improve overall energy efficiency. Such innovations align with the global push toward sustainable and multifunctional energy technologies [148].

In essence, this study not only identifies a high-performance lead-free double perovskite but also establishes a methodological blueprint for future comparative materials research, paving the way for next-generation energy harvesting solutions.

6. CONCLUSION

The present study delivers a comprehensive and comparative first-principles investigation into the optoelectronic and thermoelectric potential of lead-free double perovskites $Cs_2AgBiBr_6$ and $Cs_2AgFeCl_6$. By employing a unified Density Functional Theory (DFT) framework combined with Boltzmann transport analysis, this work bridges a critical gap in the literature where these materials have rarely been evaluated under identical computational conditions for dual-function energy applications. The findings not only validate the structural and electronic reliability of these compounds but also establish a clear performance hierarchy grounded in quantitative evidence.

From a structural perspective, both materials demonstrate excellent crystallographic stability, with optimized lattice parameters closely matching experimental values (deviation <1%). However, $Cs_2AgFeCl_6$ exhibits a more negative formation energy (−2.62 eV) compared to $Cs_2AgBiBr_6$ (−2.35 eV), indicating superior thermodynamic stability. This enhanced stability is attributed to stronger Fe–Cl bonding interactions and a more compact lattice configuration, which also plays a pivotal role in influencing phonon behavior and thermal transport. The electronic structure analysis reveals indirect bandgaps of approximately 1.85 eV for $Cs_2AgBiBr_6$ and 1.62 eV for $Cs_2AgFeCl_6$. The reduced bandgap in $Cs_2AgFeCl_6$ is mechanistically linked to strong Fe-d and Cl-p orbital hybridization, which lowers the conduction band minimum and enhances charge carrier mobility. This bandgap positioning aligns more favorably with the visible region of the solar spectrum, making $Cs_2AgFeCl_6$ a more efficient light absorber for photovoltaic applications.

Optical investigations further reinforce this advantage, with $Cs_2AgFeCl_6$ exhibiting a red-shifted absorption edge and stronger overlap with high-intensity regions of the solar spectrum. This translates into improved photon harvesting capability and reduced

optical losses. In parallel, thermoelectric analysis over a wide temperature range (300–800 K) reveals that $Cs_2AgFeCl_6$ consistently outperforms its counterpart, achieving a higher Seebeck coefficient (~320 μV/K) and an elevated figure of merit (ZT ≈ 0.89), compared to ~280 μV/K and ZT ≈ 0.72 for $Cs_2AgBiBr_6$. The integration of these multi-domain properties clearly identifies $Cs_2AgFeCl_6$ as the superior material in terms of overall performance. Its ability to simultaneously deliver strong optoelectronic response and high thermoelectric efficiency positions it as a promising candidate for next-generation multifunctional energy devices, particularly in hybrid systems that aim to harvest both solar and thermal energy.

Key Takeaways

- The first major takeaway is that structural compactness and stronger ionic bonding in $Cs_2AgFeCl_6$ significantly enhance its thermodynamic stability, making it more suitable for long-term device applications.
- The second key insight is that orbital hybridization, specifically between Fe-d and Cl-p states, plays a decisive role in reducing the bandgap and improving electronic conductivity, thereby directly influencing optoelectronic performance.
- The third important conclusion is that $Cs_2AgFeCl_6$ demonstrates superior optical absorption characteristics due to its better alignment with the solar spectrum, which enhances its photovoltaic potential.
- The fourth takeaway highlights the thermoelectric advantage of $Cs_2AgFeCl_6$, where higher Seebeck coefficient and improved carrier transport lead to a significantly higher ZT value.
- The fifth key finding is that a unified computational framework is essential for accurate comparative analysis, as it eliminates inconsistencies arising from methodological variations commonly observed in literature.
- The sixth and final takeaway is that multifunctionality combining optoelectronic and thermoelectric properties within a single material is not only achievable but also strategically advantageous for future energy systems.

REFERENCES

1. W. Irungu M. Kahura, "Comparative First-Principles Study of Lead-Free $Cs_2AgB'Br_6$ (B′ = Bi, Sb, In) Double Perovskites for Photovoltaic Applications," Dec. 2025.
2. B. Aftab Alam and M. Aslam, "Anion/cation substitution in lead-free halide double perovskite films: Towards bandgap optimization," J. Nanomater. Energy Eng., Mar. 2023. https://doi.org/10.1680/jnaen.23.00001
3. T. Atsue, I. B. Ogunniranye, and E. O. Oyewande, "Investigation of material properties of halide mixed lead-free double perovskite for optoelectronic applications using first-principles study," Mater. Sci. Semicond. Process., Oct. 2021. https://doi.org/10.1016/j.mssp.2021.105963
4. Q. Li, Y. Wang, W. Pan, W. Yang, and B. Zou, "High pressure band gap engineering in lead-free $Cs_2AgBiBr_6$ double perovskite," Angew. Chem. Int. Ed., Oct. 2017. https://doi.org/10.1002/anie.201708684
5. Q. Li, Y. Wang, W. Pan, W. Yang, and B. Zou, "High pressure band gap engineering in lead-free $Cs_2AgBiBr_6$ double perovskite," Angew. Chem., Oct. 2017. https://doi.org/10.1002/ange.201708684
6. N. Al Aqtash, S. M. Al Azar, A. Y. Al-Reyahi, A. Mufleh, and M. Maghrabi, "First-principles calculations to investigate structural, mechanical, electronic, optical, and thermoelectric properties of novel cubic double perovskites $X_2AgBiBr_6$ (X = Li, Na, K, Rb, Cs) for optoelectronic devices," Mol. Phys., Aug. 2023. https://doi.org/10.1080/08927022.2023.2251604
7. F. Ji, J. Klarbring, F. Wang, W. Ning, and L. Wang, "Lead-free halide double perovskite $Cs_2AgBiBr_6$ with decreased bandgap," Angew. Chem., May 2020. https://doi.org/10.1002/ange.202005568
8. S. Beniwal, A. Kumar, R. Kumar, A. Suhail, and M. Bag, "Tuning conductivity of lead-free $Cs_2AgBiBr_6$ double perovskite ternary composite with PEDOT:PSS and carbon black for supercapacitor application," J. Phys. Chem. C, Jun. 2023. https://doi.org/10.1021/acs.jpcc.3c02157
9. C. Kursun, M. M. Hasan, A. Kabir, I. D. Parrey, and A. Khursheed, "Enhancing the photophysical properties of absorption and luminescence in lightly doped halide double perovskite nanomaterials," Nano Mater. Sci., Aug. 2025. https://doi.org/10.1016/j.nxmate.2025.101032
10. M. A. Rahman, M. S. H. Saikot, R. Rafiu, M. S. I. Ria, and Z. Bayhan, "Comprehensive first-principles investigation of A_2GeX_6 double halide perovskites for energy and optoelectronic applications," Energy Technol., Jan. 2026. https://doi.org/10.1002/ente.202502073
11. Almalki and S. Alotaibi, "First-principles simulation for optoelectronic characteristics and structural relaxation of lead-free halide double perovskites," J. Electron. Mater., Apr. 2025. https://doi.org/10.1007/s11664-025-12009-z
12. Y. Bahloul, "Lead-free halide double perovskites Rb_2AgYF_6 and Rb_2AgYI_6: Stability and optoelectronic properties," Nov. 2025. https://doi.org/10.13140/RG.2.2.10341.87525
13. S. Gupta, D. Maurya, S. K. Srivastava, U. K. Pareek, and A. P. Srivastava, "Unveiling pressure-driven transitions in $Cs_2AgBiBr_6$: Insights from DFT into a lead-free solar perovskite," Jan. 2026. https://doi.org/10.26565/2312-4334-2026-1-43

14. D. Choudhary, M. Kaur, G. Sharma, R. Palsaniya, and S. Loyalka, "Impact of halide variation on the optoelectronic properties of double perovskites," Sci. Rep., Sep. 2025. https://doi.org/10.1038/s41598-025-98686-6
15. T. Zhang, Y.-N. Wu, and S. Chen, "Bandgap engineering through halide double perovskite alloys: A high-throughput first-principles study," Phys. Status Solidi RRL, Jul. 2021. https://doi.org/10.1002/pssr.202100343
16. S. D. Dipta, J. Islam, S. Gouadria, M. S. Ahmad, and A. El-Rayyes, "First-principles investigation of Cs_2NaGaX_6 (X = F, Cl, Br) for optoelectronic applications," New J. Chem., Mar. 2026. https://doi.org/10.1039/D5NJ04533A
17. X. Zhao, J. Luo, H. Sun, C. Liu, and H. Tan, "Design of In^{3+}-doped $Cs_2AgBiCl_6$ lead-free halide double perovskite with efficient visible absorption," Korean J. Chem. Eng., Nov. 2025. https://doi.org/10.1007/s11814-025-00602-1
18. N. K. Tailor, N. Parikh, P. Yadav, and S. Satapathi, "Dielectric relaxation and polaron hopping in $Cs_2AgBiBr_6$ halide double perovskites," J. Phys. Chem. C, Jun. 2022. https://doi.org/10.1021/acs.jpcc.2c02073
19. M. S. Khan, A. Khan, F. Aljubairi, A. Mishra, and S. Ahmad, "Ultrasonic-assisted synthesis of $Cs_2AgBiBr_6$ nanocrystals for photovoltaic and photocatalytic applications," J. Nanosci. Nanotechnol., May 2025. https://doi.org/10.1166/jno.2025.3756
20. Benkatlane, D. Rached, M. Caid, H. Rached, and E. Deligoz, "Lead-free $Cs_2(Cd/Sn)BeCl_6$ double perovskites: A first-principles study," Phys. Status Solidi B, Jul. 2025. https://doi.org/10.1002/pssb.202500019
21. L. Wang, L. Li, J. Zhang, S. Zhong, and B. Xu, "First-principles investigation of the structural stability and physical properties of lead-free Ge-based halide perovskites," Crystals, Sep. 2025. https://doi.org/10.3390/cryst15090793
22. J. Wang, L. Wang, F. Wang, S. Jiang, and H. Guo, "Pressure-induced bandgap engineering of $(NH_4)_2SnBr_6$," Phys. Chem. Chem. Phys., Sep. 2021. https://doi.org/10.1039/D1CP03267D
23. L. Wang, L. Li, J. Zhang, S. Zhong, and B. Xu, "First-principles investigation of lead-free Ge-based halide perovskites," Aug. 2025. https://doi.org/10.20944/preprints202508.1247.v1
24. T. Ahmed, A. P. Arko, M. S. Islam, M. N. H. Shefat, and D. Basak, "First-principles investigation of thallium-based double perovskites A_2AlTlI_6," Mar. 2026.
25. S. Wu, S. Ma, C. Zhao, S. Li, and M. Ye, "Pressure-modulated bandgap and optoelectronic properties in Cs_2TeCl_6," Acta Phys. Sin., Jan. 2025. https://doi.org/10.7498/aps.74.20250693
26. M. A. Hadi, M. N. Islam, and J. Podder, "Indirect to direct bandgap transition in $Cs_2AgBiBr_6$ via antisite defects," RSC Adv., May 2022. https://doi.org/10.1039/d1ra06308a
27. S. Adhikari and P. Johari, "Monovalent-cation transmutation effects on lead-free halide double perovskites," Phys. Rev. Mater., Jul. 2023. https://doi.org/10.1103/PhysRevMaterials.7.075401
28. S. Ullah, F. Rasheed, M. Al-Rasheidi, F. Khan, and J. Khan, "Theoretical and experimental investigation of $Cs_2AgBiBr_{5\cdot5}I_{0\cdot5}$," Sol. Energy, Nov. 2025. https://doi.org/10.1016/j.solener.2025.114176
29. H. Chen, C. Li, W. Zhou, J. Wen, and M. Ma, "Designing and optimizing the lead-free double perovskite $Cs_2AgBiI_6/Cs_2AgBiBr_6$ bilayer perovskite solar cell," Sol. Energy, Nov. 2024. https://doi.org/10.1016/j.solener.2024.113087
30. Z. Zhang, C. Xiong, C. Chen, S. Wang, and Y. Cai, "Machine learning-guided design and strain engineering of lead-free double perovskites for enhanced optoelectronic performance," Jan. 2026. https://doi.org/10.2139/ssrn.6501988
31. W. Meng, X. Wang, Z. Xiao, J. Wang, and D. B. Mitzi, "Parity-forbidden transition as an origin of the large optical bandgap of $Cs_2AgInCl_6$ lead-free halide double perovskite," Feb. 2017. https://doi.org/10.48550/arXiv.1702.03593
32. T. Rahman, I. A. Ovi, S. M. Shamsuddoha, and S. Bandhya, "First-principles investigation of radium-based halide perovskites: A DFT study," AIP Adv., Feb. 2026. https://doi.org/10.1063/5.0299446
33. K. Astakala and N. Lee, "From optoelectronics to scintillation applications: The versatility of lead-free halide double perovskites," Mater. Horiz., Jun. 2025. https://doi.org/10.1039/D5MH00573F
34. P. Asif, A. Chetia, D. Saikia, and S. Sahu, "A comprehensive theoretical investigation of $Cs_2AgBi_{0\cdot75}Sb_{0\cdot25}Br_6$ solar cell using SCAPS-1D," Jun. 2025. https://doi.org/10.1007/s44291-025-00085-8
35. L. Cheng, L. Huang, M. Sun, Y. Meng, and Y. Li, "Ultralow dark current soft X-ray detectors based on $Cs_2AgBiBr_6$," J. Semicond., Jan. 2026. https://doi.org/10.1088/1674-4926/25070009
36. M. F. Rahman, M. B. Hossain, M. R. H. Pramanik, T. A. Galib, and M. M. Tasdid, "Exploring Rb_2CuBiI_6 double perovskite through first-principles for optoelectronic applications," J. Inst. Eng. India Ser. B, Dec. 2025. https://doi.org/10.1007/s12648-025-03905-5
37. Srivastava, "A comparative study of optoelectronic behavior of Cs-based halide double perovskites for solar cell applications," Feb. 2025. https://doi.org/10.1201/9781003558712-13
38. R. Rafiu, M. S. Hasan, A. El-Rayyes, I. A. Apon, and M. Shkir, "Exploring A_2CeCl_6 double perovskites via first-principles and device simulation," J. Phys. Chem. Solids, Aug. 2025. https://doi.org/10.1016/j.jpcs.2025.113126

39. W. Ning, X. Zhao, J. Klarbring, S. Bai, and F. Ji, "Thermochromic lead-free halide double perovskites," Adv. Funct. Mater., Jan. 2019. https://doi.org/10.1002/adfm.201807375
40. M. A. Jehangir, S. Rabhi, R. Makhloufi, A. I. Shimul, and A. N. Khan, "Bridging first-principles calculations and device simulations of A_3GaI_6 double perovskites," RSC Adv., Mar. 2026. https://doi.org/10.1039/d5ra09544a
41. C. Lan, S. Zhao, J. Luo, and F. Ping, "First-principles study of anion diffusion in lead-free halide double perovskites," Phys. Chem. Chem. Phys., Sep. 2018. https://doi.org/10.1039/C8CP04150D
42. Laassouli, M. Karouchi, A. Ejjabli, and A. El Hamza Errahoui, "Halide-driven tuning in K_2AgSbX_6 double perovskites: A DFT study," J. Mol. Model., Mar. 2026. https://doi.org/10.1007/s00894-026-06669-9
43. P. R. Varadwaj and H. M. Marques, "Physical and optoelectronic features of $A_2AgRhBr_6$ double perovskites," J. Mater. Chem. C, Aug. 2020. https://doi.org/10.1039/D0TC02501A
44. X. Zhan, X. Chen, C. Li, T. Jin, and Y. Wang, "Can lead-free double halide perovskites serve as proper photovoltaic absorber?" J. Phys. Chem. Lett., Nov. 2023. https://doi.org/10.1021/acs.jpclett.3c02663
45. Sharma, H. Gulupalli, S. Thada, S. Jain, and R. K. Goyal, "Low-temperature synthesis of $Cs_2AgBiBr_6$ double perovskite ink," J. Nanomater. Energy Eng., Dec. 2022. https://doi.org/10.1680/jnaen.23.00004
46. N. P. Mathew, N. R. Kumar, and R. Radhakrishnan, "First principle study of $Cs_2AgInCl_6$ double perovskite," Mater. Today Proc., Apr. 2020. https://doi.org/10.1016/j.matpr.2020.03.489
47. Rahman, M. A. Torres, and M. Idowu, "Hybrid interface engineering in lead-free double perovskite solar cells," Sep. 2025. https://doi.org/10.5281/zenodo.17373025
48. F. L. Ferreira, L. F. Magalhães, T. A. S. Carvalho, and M. A. Schiavon, "Lead-free halide double perovskites nanomaterials: Fundamentals and advances," J. Braz. Chem. Soc., Jan. 2024. https://doi.org/10.21577/0103-5053.20240092
49. S. Mehmood, S. R. Khan, Z. Ali, A. Ahmad, and N. Khan, "Optoelectronic properties and solar cell performance of lead-free halide perovskites," Phys. Scr., Jun. 2025. https://doi.org/10.1088/1402-4896/ade349
50. N. M. Rahman, M. Adnaan, D. Adhikary, M. Islam, and M. K. Alam, "DFT-based study of optoelectronic properties of doped perovskites," Comput. Mater. Sci., Jul. 2018. https://doi.org/10.1016/j.commatsci.2018.04.048
51. M. Ghasemi, M. Hao, M. Xiao, P. Chen, and D. He, "Lead-free metal-halide double perovskites: From optoelectronic properties to applications," Nanophotonics, Dec. 2020. https://doi.org/10.1515/nanoph-2020-0548
52. Y. A. Sade, G. Babaji, A. Lawal, and A. S. Gidado, "First-principles study of Ba_3AsCl_3 perovskite for optoelectronics," Dec. 2025. https://doi.org/10.56919/usci.2544.008
53. H. Guo, M. He, Y. Jiang, H. Li, and J. Zhang, "Structural and optoelectronic properties of $Cs_2AgInCl_2$ under high pressure," Acta Phys. Sin., Jan. 2025. https://doi.org/10.7498/aps.74.20250613
54. W. Zheng, X. Gan, D. Du, Y. Wang, and S. Dai, "First principle study of cesium-based lead-free halide double perovskites," J. Mater. Sci. Technol., May 2023. https://doi.org/10.1007/s11595-023-2727-z
55. T. Li, X. Zhao, D. Yang, M.-H. Du, and L. Zhang, "Intrinsic defect properties in halide double perovskites," Aug. 2018. https://doi.org/10.48550/arXiv.1808.05330
56. M. Roknuzzaman, J. A. Alarco, H. Wang, and K. Ostrikov, "Structural and optoelectronic properties of antimony-copper hybrid double perovskites," Comput. Mater. Sci., Jan. 2021. https://doi.org/10.1016/j.commatsci.2020.110009
57. N. S. Alsaiari, I. Ahmed, S. Hanf, R. M. M., and M. Kundlas, "Unveiling the potential of X_2RbAsI_6 halide double perovskites," J. Mater. Sci., Apr. 2025. https://doi.org/10.1007/s10904-025-03746-z
58. Das and M. R. Amin, "Designing high-performance halide double perovskites X_2AgIrI_6 for energy applications," Dec. 2025. https://doi.org/10.13140/RG.2.2.32084.26245
59. Das and M. R. Amin, "Designing High-Performance Halide Double Perovskites X_2AgIrI_6 (X = Rb, Cs) for Energy Conversion Applications: A First-Principles Perspective Presented by Apu," Research, Dec. 2025. https://doi.org/10.13140/RG.2.2.32084.26245
60. M. Muddassir, S. S. A. Gillani, A. K. Alanazi, and M. Shakil, "Evaluation of lead-free halide double perovskites A_2GaScI_6 (A = Li, Rb, Cs) for thermoelectric and optoelectronic applications: a first-principles approach," J. Mater. Sci., Dec. 2025. https://doi.org/10.1007/s12034-025-03489-0
61. T. Tesfamichael, M. Roknuzzaman, C. Zhang, K. Ostrikov, and A. Du, "Electronic and optical properties of lead-free hybrid double perovskites for photovoltaic and optoelectronic applications," Sci. Rep., Jan. 2019. https://doi.org/10.1038/s41598-018-37132-2
62. ul Haq, T. S. Ahmad, A. Ahmad, B. S. Almutairi, and M. Amin, "A_2LiGaI_6 (A = Cs, Rb): New lead-free and direct bandgap halide double perovskites for IR application," Heliyon, Oct. 2023. https://doi.org/10.1016/j.heliyon.2023.e21702
63. Bouzgou, Y. Djaballah, R. Beddiaf, H. Righi, and L. Bennour, "First-principles investigation of structural, electronic, elastic, and optical properties of lead-free Cs_2KCoX_6 (X = F, Cl, Br, I) double perovskites," J. Phys. D Appl. Phys., Dec. 2025. https://doi.org/10.1088/1361-651X/ae21fb

64. Wang and J. Wang, "Prediction of Bandgap and Key Feature Analysis of Lead-Free Double Perovskite Oxides Based on Deep Learning," Molecules, Mar. 2026. https://doi.org/10.3390/molecules31061032
65. S. Jbara, H. T. Naeem, J. Munir, M. A. Saeed, and T. Akhter, "Investigation of the Lead-Free Perovskites $AlSnX_3$ (X = Cl, Br, I) for Optoelectronic Applications: A First-Principles Analysis," J. Mater. Sci., Jul. 2025. https://doi.org/10.1007/s10904-025-03933-y
66. T. Geng, M. Wang, Z. Chen, Y. Li, and A. Zhang, "Pressure Effect on All-Inorganic Lead-Free Halide Perovskite Materials: Structural and Optical Properties," ChemNanoMat, Apr. 2025. https://doi.org/10.1002/cnma.202400677
67. M. Ponniah and P. Nallamuthu, "First-principles study of lead-free halide double perovskites Cs_2AsNaX_6 (X = F, Cl, Br) for multifunctional applications," Phys. Scr., Nov. 2025. https://doi.org/10.1088/1402-4896/ae1eb6
68. Klarbring, O. Hellman, I. A. Abrikosov, and S. I. Simak, "Anharmonicity and Ultra-Low Thermal Conductivity in Lead-Free Halide Double Perovskites," Preprint, Dec. 2019. https://doi.org/10.48550/arXiv.1912.05351
69. Babaei, V. Ahmadi, and G. Darvish, "Opto-electro-mechanical properties of lead-free hybrid double perovskites Cs_2AgSbX_6 (X = Cl, Br, I) for solar cells: A first-principles study," J. Phys. Chem. Solids, Jul. 2022. https://doi.org/10.1016/j.jpcs.2022.110880
70. Al-Hmoud, B. Gul, Z. Ullah, M. S. Khan, and S. M. Aziz, "The Electronic, Optical, and Thermoelectric Nature of Cs_2InAgX_6 (X = Cl, F) Halide Perovskites: For Advanced Optoelectronic Applications," Biointerface Res., Dec. 2025. https://doi.org/10.1002/bio.70374
71. Klarbring, O. Hellman, I. A. Abrikosov, and S. I. Simak, "Anharmonicity and Ultra-Low Thermal Conductivity in Lead-Free Halide Double Perovskites," Preprint, Dec. 2019. https://doi.org/10.48550/arXiv.1912.05351
72. F. Elmourabit, Y. Essakali, F. Id Ouissaaden, H. Kamel, and M. Aoutoul, "Electronic Structure and Optical Response of $Cs_2AgSbBr_6$: A Lead-Free Double Perovskite for Sustainable Photovoltaics," E3S Web Conf., Mar. 2026. https://doi.org/10.1051/e3sconf/202669802001
73. U. Haq, R. Ghodhbani, A. Ali, N. Al-Hoshani, and I. Khan, "First principle studies of the lead-free all-inorganic halide double perovskites Cs_3InX_6 (X = Cl, Br and I)," Int. J. Mod. Phys. B, Apr. 2025. https://doi.org/10.1142/S0217979225501723
74. F. Afzaal, R. Jalil, I. Riaz, N. Muhammad, and G. Murtaza, "First-principles insights into lead-free K_2AgRhX_6 (X = F, Cl, Br, I) halide double perovskites as stable platforms for next-generation optoelectronic and energy conversion devices," J. Mol. Model., Feb. 2026. https://doi.org/10.1007/s00894-025-06626-y
75. Tower, F. S. Razavi, J. Dion, J. Nuss, and R. K. Kremer, "Low-temperature structural instabilities of the halide double perovskite $Cs_2AgBiBr_6$ investigated via x-ray diffraction and infrared phonons," Preprint, May 2025. https://doi.org/10.48550/arXiv.2505.10563
76. Feng, X. Luo, Q. Zhao, C. Wu, and T. Hu, "Structural, Electronic, Optical, and Mechanical Properties of Cu(I)Au(III)-Based Double Perovskites: A First-Principles Study," Phys. Status Solidi RRL, Jun. 2023. https://doi.org/10.1002/pssr.202300128
77. S. H. Shah, M. Alomar, M. Al Huwayz, W. M. Girma, and A. Safeen, "First-principles study of $X_2TlAgCl_6$ (X = K, Rb, Cs) double perovskites for high-performance optoelectronic and thermoelectric devices," Sci. Rep., Jan. 2026. https://doi.org/10.1038/s41598-026-36650-8
78. Y. Cui, X. Wang, X. Chen, Y. Wen, and S. Zhao, "ns^2-containing vacancy-ordered double perovskites for optoelectronic applications: A first-principles investigation," Solid State Commun., Jul. 2021. https://doi.org/10.1016/j.ssc.2021.114462
79. M. Hasan, N. Hasan, and A. Kabir, "DFT studies of the role of anion variation in physical properties of $Cs_2NaTlBr_6{-}xCl_x$ mixed halide double perovskites for optoelectronics," R. Soc. Open Sci., Apr. 2025. https://doi.org/10.1098/rsos.241680
80. Dey, B. Roose, and S. D. Stranks, "Optoelectronic Properties of Low-Bandgap Halide Perovskites for Solar Cell Applications," Adv. Mater., Aug. 2021. https://doi.org/10.1002/adma.202102300
81. M. M. Hasan, M. A. Sarker, M. B. Mansur, M. R. Islam, and S. Ahmad, "Pressure-Induced Structural, Electronic, Optical, and Mechanical Properties of Lead-Free $GaGeX_3$ (X = Cl, Br, I) Perovskites: First-Principles Calculation," Heliyon, Jul. 2024. https://doi.org/10.1016/j.heliyon.2024.e34824
82. U. Haq, A. Abdelkader, Y. A. H. Obaidat, R. Ghodhbani, and A. H. Ismail, "First-Principles Investigation of Optoelectronic Structure and Thermodynamic Properties of Ruddlesden-Popper Halide Perovskites for Optoelectronic Applications," J. Mater. Sci., Aug. 2024. https://doi.org/10.1007/s10904-024-03338-3
83. S. S. I. Almishal and O. Rashwan, "First-principles investigation of lead-free trigonal $CsGeI_3{-}xBr_x$ mixed-halide perovskite system for optoelectronic applications: Electronic and optical properties," Mater. Sci. Semicond. Process., Nov. 2022. https://doi.org/10.1016/j.mssp.2022.107017
84. Dixit, J. A. Abraham, K. Fatima, R. Sharma, and P. Kumari, "Tailoring the Optoelectronic and Thermoelectric Properties of Lead-Free Double Perovskites K_2NaBiZ_6 (Z = Br, I) for Renewable Energy Applications: A First-Principles Density

Functional Theory Investigation," Energy Technol., Nov. 2025. https://doi.org/10.1002/ente.202501552
85. S. Ghosh, H. Shankar, and P. Kar, "Recent Development of Lead-Free Halide Double Perovskites: A New Superstar in Optoelectronic Field," Mater. Adv., Mar. 2022. https://doi.org/10.1039/D2MA00071G
86. Islam, M. H. Islam, and M. H.-U.-R. Rashid, "Kinetically controlled halide exchange for tailoring bandgap and optoelectronic properties of hybrid perovskite microcrystals," Phase Transitions, Dec. 2025. https://doi.org/10.1080/14328917.2025.2601642
87. X. Xiao, J. Wang, D. Li, K. Kang, and H. Zhu, "Electronic Structure and Optical Properties of ABI_3 Inorganic Lead-Free Halide Perovskites: A DFT + U Study," Phys. Status Solidi B, Mar. 2026. https://doi.org/10.1002/pssb.202500536
88. M. Barua, M. Y. H. Khan, M. Z. Hasan, and J. U. Ahamed, "Halogen Engineering in Lead-Free Mg_3PX_3 Perovskites: A First-Principles Investigation for UV to IR Optoelectronic and Photovoltaic Applications," Coord. Chem. Rev., Jan. 2026. https://doi.org/10.1016/j.cocom.2026.e01220
89. H. Ahmed, S. Mukhtar, and S. Agathopoulos, "First-Principles Study on the Physical Properties of Al-based Wide Bandgap Perovskites $Cs_3AlI_xBr_{6-x}$ for Optoelectronic Applications," Semicond. Sci. Technol., Jan. 2025. https://doi.org/10.1088/1361-6641/ada986
90. Chakraborty, S. D. Dipta, T. Chakraborty, and M. R. Islam, "Comprehensive First-Principles Investigation of the Structural, Electronic, Phonon, and Optical Properties of Lead-Free Halide Double Perovskites Cs_2GeX_6 (X = F, Cl, Br, I)," in Proc. IEEE EICT, Dec. 2025. https://doi.org/10.1109/EICT68394.2025.11355602
91. M. M. Hasan and A. Kabir, "Tuning the Physical Properties of Lead-Free Halide Double Perovskite Cs_2MInCl_6 (M = Na, K) via Cu Doping for Optoelectronic Applications: A DFT Investigation," J. Phys. Chem. C, Dec. 2023. https://doi.org/10.1021/acs.jpcc.3c05891
92. Bibi, I. Lee, Y. Nah, O. Allam, and H. Kim, "Lead-free halide double perovskites: Toward stable and sustainable optoelectronic devices," Mater. Today, Jan. 2021. https://doi.org/10.1016/j.mattod.2020.11.026
93. F. Ji, F. Wang, L. Kobera, S. Abbrent, and J. Brus, "The atomic-level structure of bandgap engineered double perovskite alloys $Cs_2AgIn_1{-}xFe_xCl_6$," Chem. Sci., Dec. 2020. https://doi.org/10.1039/D0SC05264G
94. M. S. Parves, M. A. B. Siddique, M. Tarekuzzaman, S. Ahmad, and M. Rasheduzzaman, "Optimized Solar Conversion Achieved with Double Halide $X_2NaIrCl_6$ (X = Rb, Cs) Perovskites for Optoelectronic and Photovoltaic Applications," Nexus, Sep. 2025. https://doi.org/10.1016/j.nexus.2025.100549
95. S. Elhadfi, J. Chenouf, Z. Arbaoui, B. Fakrach, and R. Abdelhai, "Probing the Optoelectronic and Thermoelectric Properties of Methylammonium Germanium Halide Perovskites $CH_3NH_3Ge(Br,Cl)_3$ within First Principles Calculations," Phys. Status Solidi B, Oct. 2025. https://doi.org/10.1002/pssb.202500382
96. Y. Wei, J. He, C. Yang, W. Yu, and J. Feng, "Accelerated Multi-Property Screening of Lead-Free Halide Double Perovskite via Transfer Learning," Adv. Funct. Mater., Jul. 2025. https://doi.org/10.1002/adfm.202514377
97. J. Diaz, S. Gallardo-Hernández, J. M. Zárate-Reyes, E. Ramos, and Y. Kudriavtsev, "Impact of alkali (Na, K, Cs) substitution on the structural, electronic and optical properties of MAPI perovskites: a first-principles approach," J. Mater. Sci., Dec. 2025. https://doi.org/10.1007/s10853-025-11936-w
98. S. Zhao, K. Yamamoto, S. Iikubo, S. Hayase, and T. Ma, "First-principles study of electronic and optical properties of lead-free double perovskites Cs_2NaBX_6 (B = Sb, Bi; X = Cl, Br, I)," J. Phys. Chem. Solids, Feb. 2018. https://doi.org/10.1016/j.jpcs.2018.02.032
99. Cappai, C. Melis, and L. Colombo, "Tailoring the transport coefficients and thermoelectric properties of $Cs_2NaYbCl_6$ perovskite by doping and nanoengineering: A first-principles based theoretical approach," Phys. Rev. Mater., Jan. 2026. https://doi.org/10.1103/729y-m77y
100. T. Atsue and O. E. Oyewande, "Theoretical Study of the Transport Properties of Cs_2NaBiX_6 [X = Br, I] Double Perovskite and its Stability for Thermoelectric Applications," USCI, Feb. 2025. https://doi.org/10.56919/usci.2541.017
101. Cappai, C. Melis, and L. Colombo, "Role of electron-phonon scattering on thermoelectric coefficients in pristine $Cs_2NaYbCl_6$ perovskite: A full DFT approach," Phys. Rev. Mater., May 2025. https://doi.org/10.1103/PhysRevMaterials.9.054605
102. T. Pandey, M.-H. Du, D. S. Parker, and L. Lindsay, "Origin of ultralow phonon transport and strong anharmonicity in lead-free halide perovskites," Mater. Today Phys., Nov. 2022. https://doi.org/10.1016/j.mtphys.2022.100881
103. W. Zheng, Q. Chen, Q. Wang, and A. Chen, "Effect of four-phonon scattering on strain-dependent thermal and thermoelectric transport of ferroelectric α-In_2Se_3 monolayer," Appl. Phys. Lett., Jul. 2025. https://doi.org/10.1063/5.0279109
104. G. A. Elbaz, W.-L. Ong, E. A. Doud, P. Kim, and D. W. Paley, "Phonon Speed, Not Scattering, Differentiates Thermal Transport in Lead Halide Perovskites," Nano Lett., Aug. 2017. https://doi.org/10.1021/acs.nanolett.7b02696

105. Y. Chen, S. Cao, C. Cao, Y. Bao, and K.-K. Song, "Insight into ultra-low lattice thermal conductivity and native defect behavior in lead-free perovskite $Cs_3Sb_2I_9$," Preprint, Jan. 2026. https://doi.org/10.2139/ssrn.6417748
106. B. Huang, J. Zheng, C. Lin, C. Lin, and G. Hautier, "Unravelling Ultralow Thermal Conductivity in Double Perovskite $Cs_2AgBiBr_6$: Dominant Wave-like Phonon Tunnelling, Strong Quartic Anharmonicity and Lattice Instability," Preprint, Aug. 2023. https://doi.org/10.21203/rs.3.rs-3197125/v1
107. P. Arko, B. Ahammed, A. K. M. M. H. Sohag, D. Basak Preeti, and T. Ahmed, "Assessing the optoelectronic and thermoelectric viability of lead-free double perovskites: A comparative DFT study of Cs/Rb-Ag-Sb and Cs-Li-In variants," Coord. Chem. Rev., Feb. 2026. https://doi.org/10.1016/j.cocom.2026.e01251
108. Esfarjani and J. Shiomi, "Fundamentals and advances in thermal transport in thermoelectric materials," MRS Bull., Aug. 2025. https://doi.org/10.1557/s43577-025-00951-6
109. Zheng, C. Lin, C. Lin, R. Guo, and B. Huang, "Strong Anharmonic Phonon Renormalization and Dominant Role of Wave-like Tunnelling of Phonons in Thermal Transport in Lead-free Halide Double Perovskites," Preprint, Jan. 2023. https://doi.org/10.48550/arXiv.2301.12273
110. J.-J. Zheng, C.-J. Li, R.-R. Ma, B.-T. Wang, and J.-J. Ma, "Bonding Hierarchy and Phonon Coherence Enhanced Ultralow Lattice Thermal Conductivity and Excellent Thermoelectric Properties in Cs_2TeI_6," Chin. Phys. Lett., Jul. 2025. https://doi.org/10.1088/0256-307X/42/8/080703
111. Z. Anam, A. Rodriguez, R. Rurali, and M. Hu, "Machine Learning Discovery of Record-Low Lattice Thermal Conductivity in Double Perovskites," Adv. Sci., Feb. 2026. https://doi.org/10.1002/advs.202515766
112. Cao, Y. Wang, Z. Xia, and J. He, "Microscopic Origin of the Ultralow Lattice Thermal Conductivity in Vacancy-Ordered Halide Double Perovskites Cs_2BX_6 (B = Zr, Pd, Sn, Te, Hf, and Pt; X = Cl, Br, and I)," Preprint, Feb. 2026. https://doi.org/10.48550/arXiv.2602.06501
113. U.-S. Pak, D.-S. Che, S.-M. Jang, and U.-G. Jong, "Theoretical insights into lattice dynamics and thermal transport properties of lead-free quadruple halide perovskite $Cs_4CuSb_2Cl_{12}$," Mater. Adv., Nov. 2025. https://doi.org/10.1039/D5MA01099C
114. B. Liao, "Nanoscale electron, phonon and spin transport in thermoelectric materials," Ph.D. dissertation, Massachusetts Institute of Technology, 2016.
115. Y. Lan, Y. Zhang, H. Zhang, P. Wang, and N. Wang, "Impact of Four-Phonon Scattering on Thermal Transport and Thermoelectric Performance of Penta-XP_2 (X = Pd, Pt) Monolayers," Nanomaterials, Sep. 2025. https://doi.org/10.3390/nano15181396
116. H. Murari, S. Ghosh, M. Kabir, and A. Kundu, "Thermal and thermoelectric transport in monolayer h-NbN: Roles of four-phonon scattering and tensile strain," Preprint, May 2025. https://doi.org/10.48550/arXiv.2505.12520
117. E. A. El Goutni, M. Batouche, H. Ferjani, T. Seddik, and D. Abdullah, "Advancing Sustainable Energy: Photocatalytic and Thermoelectric Properties of Cs_2MBr_6 Double Perovskites (M = Re^{4+}, W^{4+}, Ru^{4+}, Os^{4+})," Inorg. Chem. Commun., Oct. 2025. https://doi.org/10.1016/j.inoche.2025.115644
118. X. Zhang, N. Liu, Q. Guo, G. Shi, and Y. Wang, "Beyond Boltzmann transport: Green–Kubo prediction of lattice thermal conductivity with machine-learned potentials," J. Chem. Phys., Feb. 2026. https://doi.org/10.1063/5.0297462
119. H. Murari and S. Ghosh, "Thermoelectric Properties of 2D-Janus Monochalcogenides: Anisotropic Electronic and Phonon Transport," Adv. Theory Simul., vol. Oct 2025, 2025. https://doi.org/10.1002/adts.202501075
120. Wang and S. Lin, "Anisotropic and Ultralow Phonon Thermal Transport in Organic-Inorganic Hybrid Perovskites: Atomistic Insights into Solar Cell Thermal Management and Thermoelectric Energy Conversion Efficiency," Adv. Funct. Mater., vol. May 2016, 2016. https://doi.org/10.1002/adfm.201600284
121. Sajjad, Q. Mahmood, N. Singh, and J. A. Larsson, "Ultralow Lattice Thermal Conductivity in Double Perovskite Cs2PtI6: A Promising Thermoelectric Material," ACS Appl. Energy Mater., vol. Nov 2020, 2020. https://doi.org/10.1021/acsaem.0c02236
122. X. Bi, X. Zhang, J. O. Morales-Ferreiro, and Z. Liu, "Anomalously dominating four-phonon scattering in pressure-dependent thermal transport in beryllium oxide," J. Appl. Phys., vol. May 2025, 2025. https://doi.org/10.1063/5.0260709
123. H. Murtaza, J. Munir, Q. Ain, H. M. Ghaithan, and A. A. A. Ahmed, "An in-depth analysis of the optoelectronics, phonon, mechanical, thermodynamic and transport attributes of lead-free K2TlInX6 (X= I, Br) double perovskites for green energies," Int. J. Mod. Phys. B, vol. Jan 2026, 2026. https://doi.org/10.1142/S021797922650044X
124. Kumbhakar, J. A. Abraham, A. Srivastava, K. L. Meena, and M. Manzoor, "Synergistic modulation of SLME and thermal transport toward promising p-type lead-free halide semiconductors In2TiX6 (X = Br, I) via first principles analysis," Int. J. Quantum Chem., vol. May 2024, 2024. https://doi.org/10.1002/qua.27424
125. Y. Zhao, S. Zeng, G. Li, C. Lian, and Z. Dai, "Lattice thermal conductivity including phonon frequency shifts and scattering rates induced by quartic anharmonicity in cubic oxide and fluoride

perovskites," Phys. Rev. B, vol. 104, Dec 2021, 2021. https://doi.org/10.1103/PhysRevB.104.224304
126. Y. Wang, N.-D. Chen, C. Yang, Z.-Y. Zeng, and C.-E. Hu, "Thermoelectric transport properties of two-dimensional materials XTe2 (X = Pd, Pt) via first-principles calculations," Acta Phys. Sin., vol. 70, Jan 2021, 2021. https://doi.org/10.7498/aps.70.20201939
127. Ji, A. Huang, Y. Huo, Y.-M. Ding, and S. Zeng, "Influence of four-phonon scattering and wavelike phonon tunneling effects on the thermal transport properties of TlBiSe2," Phys. Rev. B, vol. 109, Jun 2024, 2024. https://doi.org/10.1103/PhysRevB.109.214307
128. Agouri, H. Ouhenou, A. Waqdim, A. Zaghrane, and E. Darkaoui, "Computational study of stability, photovoltaic, and thermoelectric properties of new inorganic lead-free halide perovskites," EPL, vol. Apr 2024, 2024. https://doi.org/10.1209/0295-5075/ad2cb7
129. R. Rafiu, M. S. H. Saikot, I. A. Apon, I. Boukris, and A. Elrayyes, "Comprehensive DFT and SCAPS-1D Study of Structural, Electronic, Optical, Mechanical, Phonon, Thermoelectric, and Photovoltaic Properties of Lead-Free Z3BrO (Z = K, Rb, Cs, and Fr) Anti-Perovskites," J. Comput. Chem., vol. Sep 2025, 2025. https://doi.org/10.1002/jcc.70221
130. J. Harter, "Advanced Deterministic Phonon Transport Techniques for Predicting Spectral Thermal Conductivity in Homogeneous and Heterogeneous Media," Ph.D. dissertation, Oct. 2019.
131. B. G. Yalcin, "Ground state properties and energy-related applications of Cs_2CaXCl_6 (X = Si, Ge) double halide perovskites: A novel DFT study," Comput. Theor. Chem., vol. Mar 2026, 2026. https://doi.org/10.1016/j.comptc.2026.115777
132. A. Jehangir, R. Khan, N. Israr, A. M. Ali, and A. R. Choudhary, "Alkali metal substitutional effect on the structural, mechanical, optoelectronic and transport properties of X2LaCuCl6 double perovskites," Sci. Rep., vol. Oct 2025, 2025. https://doi.org/10.1038/s41598-025-20948-0
133. J. Zhou, B. Liao, and G. Chen, "First-principles calculations of thermal, electrical, and thermoelectric transport properties of semiconductors," Semicond. Sci. Technol., vol. 31, Mar 2016, 2016. https://doi.org/10.1088/0268-1242/31/4/043001
134. T. Yue, B. Xu, Y. Zhao, S. Meng, and Z. Dai, "Ultra-low lattice thermal conductivity and anisotropic thermoelectric transport properties in Zintl compound β-K2Te2," Phys. Chem. Chem. Phys., vol. Feb 2022, 2022. https://doi.org/10.1039/D1CP05248A
135. F. K. Alshammari, A. A. Alatawi, A. Jebnouni, A. S. Aljaloud, and T. Alkathiri, "Photo-activated Charge Transport and Unified Mechanism of Self-Trapped Excitons in $Cs_2NaInCl_6$ Double Perovskite," Research Square, vol. Mar 2026, 2026. https://doi.org/10.21203/rs.3.rs-9118340/v1
136. F.-Y. Xu, D. Wang, Z.-Y. Zeng, Z.-G. Li, and X.-R. Chen, "Thermal transport and thermoelectric properties of alkali-metal telluride Na2Te from first-principles study," Solid State Commun., vol. Jul 2022, 2022. https://doi.org/10.1016/j.ssc.2022.114890
137. H. Ke, J. Xian, R. Zhou, Y. Xu, and X. Lin, "Interplay of Phonon Scattering and Interfacial Coupling in Thermal Transport of MoTe2," Small, vol. Nov 2025, 2025. https://doi.org/10.1002/smll.202510993
138. Y. Han, X. Liu, X. Liu, L. Chen, and L.-M. Wu, "Lead-Doping Enabled Band Engineering and Phonon Transport Modulation: Key to High-Performance Thermoelectric AgSbTe2," Angew. Chem. Int. Ed., vol. Apr 2026, 2026. https://doi.org/10.1002/anie.2554196
139. H. V. Kumar Pandey, A. Dixit, A. Aziz, and S. K. Kang, "Distorted polyhedral architecture enabled high thermoelectric performance of columnar double halide perovskites Cs2AgPdCl5 and Cs2AgPtCl5," arXiv preprint, vol. Feb 2026, 2026. https://doi.org/10.48550/arXiv.2602.10789
140. L. Yan, L. Zhao, C. Zhao, and S. Lin, "Theoretical Understanding of Thermoelectric Energy Conversion Efficiency in Lead-Free Halide Double Perovskites Showing Intrinsic Defect Tolerance," Appl. Therm. Eng., vol. Jul 2022, 2022. https://doi.org/10.1016/j.applthermaleng.2022.119024
141. H. Wei, W. Xu, X. Jin, X. Ding, and L. Shi, "Ultralow lattice thermal conductivity and glass-like thermal transport induced by double stacking faults in monolayer MS2 (M = Mo, W)," J. Appl. Phys., vol. Sep 2025, 2025. https://doi.org/10.1063/5.0292424
142. Dixit, J. A. Abraham, K. Fatima, R. Sharma, and P. Kumari, "Tailoring the Optoelectronic and Thermoelectric Properties of Lead-Free Double Perovskites K2NaBiZ6 (Z = Br, I) for Renewable Energy Applications: A First-Principles Density Functional Theory Investigation," Energy Technol., vol. Nov 2025, 2025. https://doi.org/10.1002/ente.202501552
143. K. Radja, L. F. Ameri, I. Drici, and F. Issad, "Investigation of structural, magneto-electronic, elastic, mechanical and thermoelectric properties of novel lead-free halide double perovskite Cs2AgFeCl6: First-principles calcuations," J. Phys. Chem. Solids, vol. May 2022, 2022. https://doi.org/10.1016/j.jpcs.2022.110795
144. L. Han, Z. Li, Z. Tang, X. Wang, and J. Li, "Notable impact of magnetic order and flat phonon mode on the thermal transport properties of 2D magnetic semiconductor CrSBr," J. Appl. Phys., vol. Nov 2025, 2025. https://doi.org/10.1063/5.0270732

145. Wang, M. Zhang, L. He, S. Kan, and R. Song, "Balancing the Competing Effects of Carrier and Phonon Transport Mechanisms to Enhance the Thermoelectric Properties of p-Type Ti2Zr2−xHf2Nb2Fe5.6Ni2.4Sb8 Double Half-Heusler Alloys via Cation Vacancy Engineering," Energy Efficient Mater., vol. Oct 2025, 2025. https://doi.org/10.1002/eem2.70170
146. H. Xie, S. Hao, J.-K. Bao, T. J. Slade, and G. J. Snyder, "All-Inorganic Halide Perovskites as Potential Thermoelectric Materials: Dynamic Cation off-Centering Induces Ultralow Thermal Conductivity," J. Am. Chem. Soc., vol. Apr 2020, 2020. https://doi.org/10.1021/jacs.0c03427
147. Mahmood, W. Al-Masry, and S. M. Ramay, "DFT investigations of optoelectronic and electronic transport properties of Li-based double perovskites for energy storage applications," Phys. Scr., vol. Jun 2023, 2023. https://doi.org/10.1088/1402-4896/acd74c
148. Khan, G. Murtaza, J. M. Asiri, M. Saeed, and A. Zeb, "Photovoltaic, photocatalytic and thermoelectric properties of X2LaAuBr6 (X = K, Rb, Cs) double perovskites," J. Mater. Sci., vol. Feb 2026, 2026. https://doi.org/10.1007/s10971-025-07068-x